Nuclear Physics and Astrophysics
Research Highlights

Detection of Dark Matter and Low-Energy Solar Neutrinos with Liquid Neon

M.G. Boulay, A. Hime, J. Lidgard, D.-M. Mei (P-23)

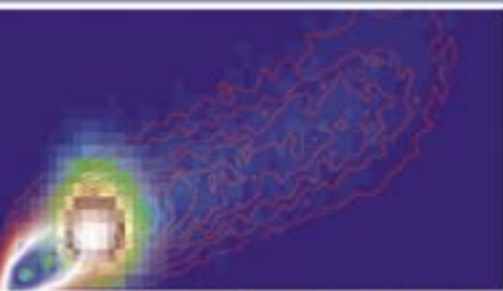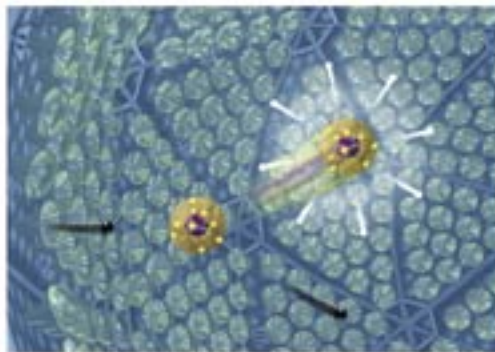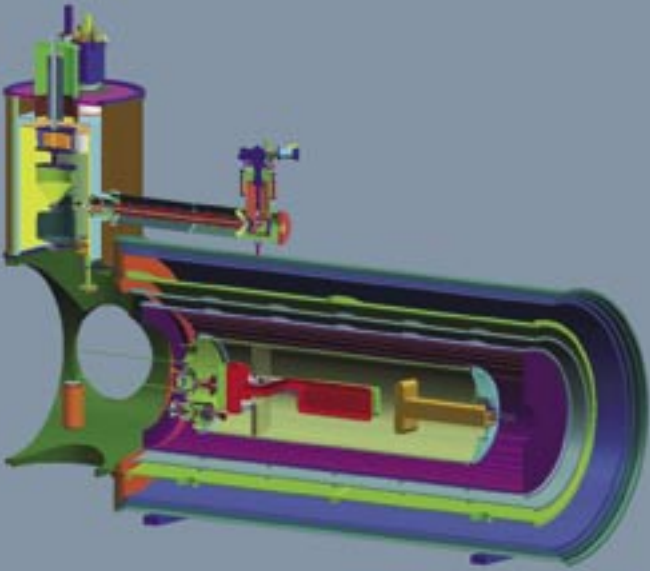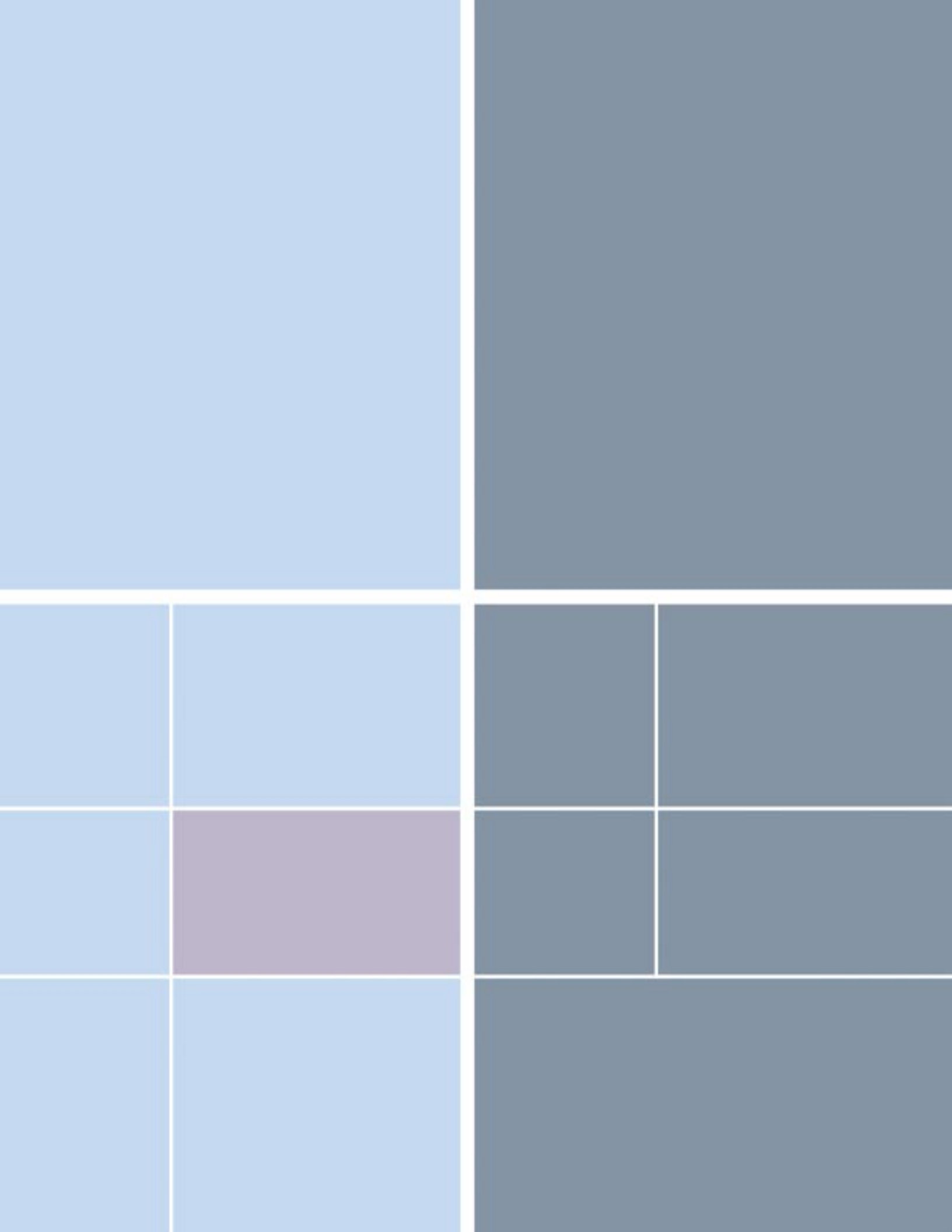The origin of dark matter in our universe and the study of low-energy solar neutrinos are two of the foremost topics in particle astrophysics. It has long been known that much of our universe is composed of an undetected form of matter, known as *dark matter*. Initial evidence for dark matter came from rotation curves of galaxy clusters and galaxies, an example of which is shown in Figure 1(b). Objects at very large distances from galactic centers are found to have velocities too large to be gravitationally bound by only the visible matter in the galaxy. Additional matter must be present to account for the fact that these objects are indeed bound by gravitational forces. A currently favored hypothesis is that dark matter consists of a new type of particle, a weakly interacting massive particle (WIMP), which has so far remained undetected.

Current searches for dark matter attempt to detect WIMPs from our galaxy's dark-matter halo through their elastic scattering on target nuclei. Because the interaction between WIMPs and matter is extremely weak, event rates in terrestrial detectors are low. Current experimental searches are limited by the total mass of target material achievable, with limits on the WIMP interaction rate on the order of events per kilogram of detector material per day. Extreme care must be taken to reduce sources of background contamination in these experiments. The goal for next-generation experiments is to improve sensitivity by several orders of magnitude, with target masses on the order of tons.
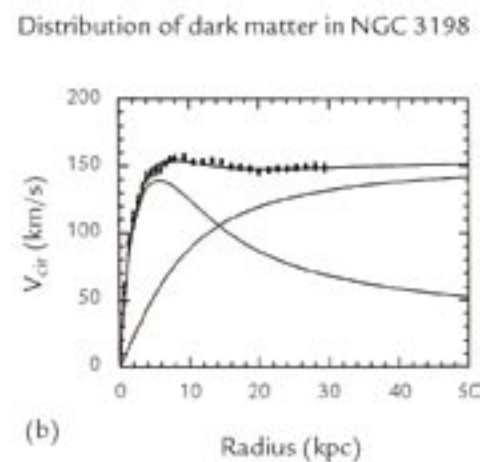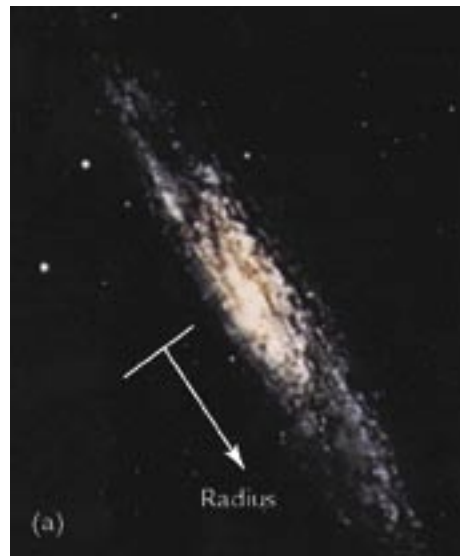

Figure 1. (a) Optical image of galaxy NGC 3198.[1] "Radius" is the distance from the galactic center. (b) Distribution of velocities versus radius.[2] The curve labeled "disk" shows the contribution from visible objects in the galactic disk. The curve labeled "halo" shows the contribution from a dark-matter halo required to explain the experimental result.

Since the experimental discovery of the neutrino by a team of LANL researchers, the field of neutrino physics has become rich with new insights into the fundamental properties of the neutrino. A wide range of the solar neutrino spectrum (Figure 2) has been probed by solar-neutrino experiments during the past four decades. LANL has played a leading role in the Sudbury Neutrino Observatory (SNO), recent results of which have conclusively shown that electron neutrinos (ν_e) emitted in the sun undergo transformation into other neutrino flavors (ν_μ, ν_τ), solving a decades-old problem of missing solar neutrinos.[3,4] Future experimental efforts on solar neutrinos will focus on very precise measurements of the lowest-energy solar neutrinos. The flux of *pp* neutrinos is very well predicted by standard models of solar evolution and is tightly constrained by the observed solar luminosity.

RESEARCH HIGHLIGHT

PHYSICS DIVISION

Measurement of this component of the solar spectrum with high precision and in real time will shed light onto both the solar models and the fundamental properties of the neutrinos themselves.

Cryogenic Low-Energy Astrophysics with Neon

The CLEAN (Cryogenic Low-Energy Astrophysics with Neon) experiment (Figure 3) will be sensitive to the low-energy pp solar neutrinos (ν_x) and to WIMP particles (χ) through their elastic scattering from electrons and neon nuclei, respectively:

$$\nu_x + e^- \rightarrow \nu_x' + e^{-'} \qquad (1)$$

$$\chi + Ne \rightarrow \chi' + Ne' \qquad (2)$$

The recoiling electrons (ν_x') or neon nuclei (Ne') lead to the production of scintillation photons in the liquid neon (approximately 15,000 photons per MeV of kinetic energy), which can then be detected by the photomultiplier tubes (PMTs). The concept of a liquid-neon scintillation detector on which this work is based was first put forward by McKinsey and Doyle.[6] The proposed experiment consists of a large volume of liquid neon surrounded by 1842 PMTs

that detect scintillation photons produced by the recoiling electrons (e$^{-'}$) or Ne' from reactions (1) and (2). A key to the CLEAN experiment is the difference in emission times of scintillation photons from reactions (1) and (2), allowing discrimination between these two reactions. At the projected sensitivity of the CLEAN experiment, low-energy solar neutrinos occur at rates much greater than the WIMP scattering rates, and separating these event types is critical to the success of the experiment. CLEAN is projected to measure the dominant pp component of the solar-neutrino flux with 1% precision.

To evaluate the detector's capability, we performed detailed Monte Carlo simulations. Nominal properties associated with the production and propagation of scintillation photons (scintillation yield, scattering lengths, etc.) and PMTs with currently achievable background levels were assumed in the simulation. PMT glass contains small traces of uranium, thorium, and potassium, which can decay and generate scintillation photons that could then be mistaken for signal events. Many of the properties of scintillation light in neon are not well known, and part of the current experimental program at LANL is to improve our knowledge of these.

Scintillation-Event-Position Reconstruction

Scintillation events from radioactive decays in the PMTs or other sources of radioactivity external to the neon are a potential background to the solar-neutrino or WIMP scintillation signals. Reducing this background to an acceptable level requires the reconstruction of scintillation-event positions based on the PMT data, which samples the scintillation photons. We have developed a new position reconstruction algorithm based on our detector simulation. The algorithm shows significant improvement over earlier geometrical reconstruction algorithms by including PMT timing information (Figure 4). The reconstruction of scintillation-event positions is critical to the success of CLEAN because it allows us to use a large target mass of neon necessary for WIMP sensitivity with a very low-energy threshold (approximately 12 keV) essentially free of PMT backgrounds.

Background Contamination

Purification of the neon is expected to reduce background contamination from internal sources of radioactivity significantly because at the very low temperature of liquid neon most impurities will bind efficiently to carbon and can thus be removed by cold traps. The PMTs and associated hardware will contain the largest amount of radioactive contamination near the inner detector volume, and these are mitigated by applying position reconstruction algorithms described above. The dominant internal source of background for CLEAN is expected to be krypton-85 because it has a relatively short half-life (approximately 11 years), decays through e$^-$ emission with energies in the same range as the ν_x neutrinos (Q-value = 687 keV), and is present in the atmosphere. Several other naturally occurring radioactive contaminants will need to be removed from the neon to achieve acceptable background levels for neutrino detection.

Figure 2. The neutrino energy spectrum from fusion reactions in the sun predicted by Bahcall and Pinsonneault.[5] Solar neutrino experiments have detected neutrinos over most of the energy range. The gallium and chlorine experiments have measured integral fluxes of neutrinos with radiochemical techniques; SNO and SuperK have detected the higher-energy neutrinos in real time. The goal for next-generation experiments is to measure with high precision and in real time the lowest-energy solar neutrinos.
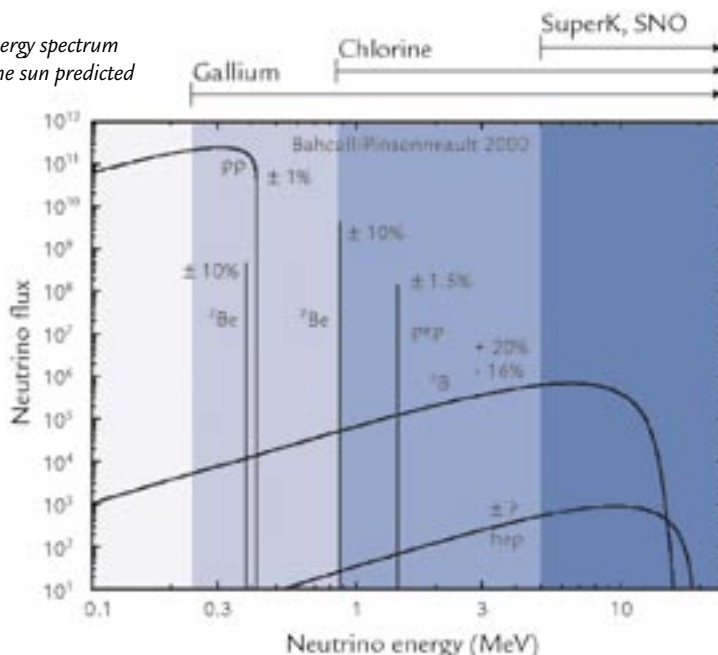
Conclusions

We have demonstrated the possibility for a simultaneous dark-matter and low-energy neutrino experiment using liquid neon, assuming nominal scintillation characteristics and background contamination levels. Assuming the required background contamination levels can be achieved, the large target mass possible with neon may lead to the best sensitivity for detecting dark-matter particles. The current research and development program at LANL focuses on providing precise measurements of some of the fundamental scintillation properties in liquid neon and achievable background contamination levels, both of which are critical to the feasibility of the experiment. A test cell of approximately 5 kg of neon is being designed to measure the precise scintillation time distribution for both electron and nuclear recoils in liquid neon. A system currently under construction will clean neon gas of impurities using cold traps, with the goal of ultimately demonstrating the background requirements needed for the full-scale detector. Studies are under way to design a small-scale prototype that could be used to further assess scintillation and background properties and provide initial limits on WIMP interactions.
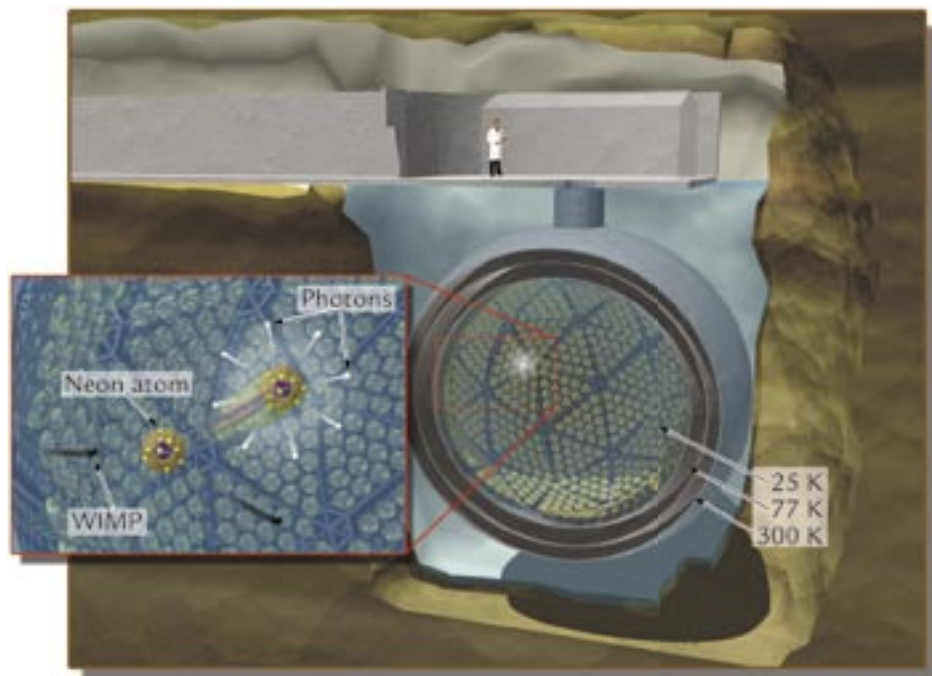

Figure 3. The CLEAN experiment. A spherical array of 1842 PMTs look inward into a large volume of liquid neon (at approximately 25 K). Elastic scattering of neutrinos or WIMP particles from electrons or neon nuclei (respectively) lead to the production of scintillation photons, which are then detected by the PMTs. Data from the PMTs are then used to reconstruct the event position and energy and statistically separate neutrino interactions, WIMP interactions, and background events.

Projected Sensitivity

By evaluating the detector response from Monte Carlo simulations and including the effects of background contamination from PMTs, internal radioactivity, and solar neutrinos, we have evaluated the ultimate sensitivity to WIMP dark matter (see Figure 5). The cross sections (interaction strength) for WIMP-nucleon interactions and the WIMP's mass are both unknown, and both affect the signal seen in CLEAN so that the sensitivity depends on these two parameters. For a 300 cm radius detector, we find an experimental sensitivity to dark matter that is several orders of magnitude better than current searches and competitive with proposed searches.

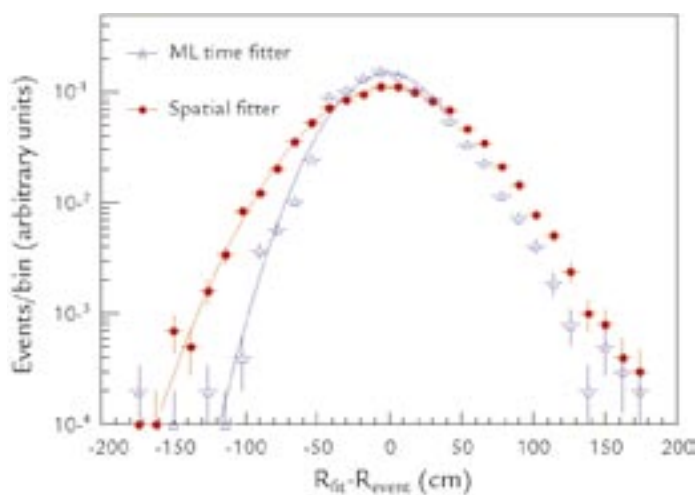Figure 4. Reconstructed position distributions for simulated low-energy events in CLEAN. Shown are the differences between the reconstructed event radius and the true event radius, which is simulated at the PMTs. The improved reconstruction algorithm, including PMT time information, significantly improves position resolution and allows us to use a much larger volume of neon for analysis of dark-matter interactions.

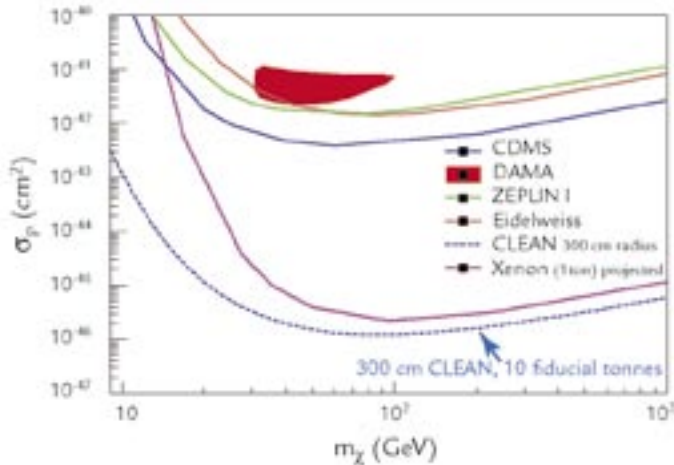# Nuclear Physics and Astrophysics Research Highlights

Figure 5. Projected sensitivity to dark-matter interactions with CLEAN and other experimental searches. The curves indicate combined exclusion regions for the WIMP's mass (m_χ) and for the WIMP-nucleon interaction strength (σ_p). The current best experimental sensitivity is from the Cryogenic Dark Matter Search (CDMS) experiment. CLEAN is projected to improve this sensitivity by four orders of magnitude. A combination of parameters above the sensitivity limit would be seen as evidence for WIMP particles in CLEAN. Data for other experiments are adapted from Reference 7.

References

1. Image of NGC 3198 adapted from *The Galaxy Catalog,* http://www.astro/princeton.edu/~freil/Gcat_htm/Catalog/CJpeg/n3198.jpg.

2. T.S. van Albada *et al.,* "Distribution of dark matter in the spiral galaxy NGC 3198," *The Astrophysical Journal* **295**, 305–313 (1985).

3. S.N. Ahmed *et al.,* (SNO Collaboration), "Measurement of the total active 8B solar neutrino flux at the Sudbury Neutrino Observatory with enhanced neutral current sensitivity," *Physical Review Letters* **92**, 181301-1–181301-6 (2004).

4. A. Hime *et al.,* "The Sudbury Neutrino Observatory—Taking physics beyond the standard model," Los Alamos National Laboratory report LA-14112-PR (2003).

5. J.N. Bahcall, M.H. Pinsonneault, and S. Basu, "Solar models: Current epoch and time dependences, neutrinos, and helioseismological properties," *Astrophysical Journal* **555**, 990–1012 (2001).

6. D.N. McKinsey and J.M. Doyle, "Liquid helium and liquid neon-sensitive, low background scintillation media for the detection of low energy neutrinos," *Journal of Low Temperature Physics* **118**, 153–165 (2000).

7. SUSY/Dark Matter Interactive Direct Detection Limit Plotter, http://dmtools.berkeley.edu/limitplots.

The World's Greatest Science Protecting America

http://www.lanl.gov/physics

Research and Development Progress toward a New Search for the Electric Dipole Moment

M. Cooper (P-25), S. Lamoreaux (P-23) representing the EDM Collaboration

Anonzero electric dipole moment of the neutron (nEDM) would be an exciting discovery because it would either solve the "strong *CP*" problem (see below) or reveal new physics beyond the standard model of electroweak interactions. In the neutron, an EDM would arise from a slight separation of positive and negative charges along the spin axis. Such a separation allows for an interaction with an applied electric field that has space-time transformations that break the time-reversal symmetry *(T)*. Symmetries of nature have their origin in conservation laws. No such law exists for the strong interaction, the origin of the nuclear force, and time reversal is expected to be broken. However, extremely sensitive searches for a nonzero nEDM have given null results. Furthermore, great experimental effort has been devoted to the search for a particle called the axion that could be the signature of an undiscovered conservation law; these searches have also provided negative results. A substantially more sensitive search for a nEDM would sharpen this conflict in our understanding.

A nonzero value for the nEDM is expected to arise at a very small value ($\sim 10^{-31}$ $e \cdot$cm) due to the violation of time reversal discovered in the strange- and bottom-quark systems. Between this (nearly) immeasurably small value and the current experimental limit of 6×10^{-26} $e \cdot$cm,[1] there exists a window for discovery of new phenomena in the standard model. Physicists have two exciting motivations to look for the nEDM: the highly popular idea of supersymmetry, which remains to be proven, predicts a value in the range

10^{-26}–10^{-28} $e \cdot$cm; the dominance of matter over antimatter in the universe resists quantitative explanation, and another source of *T* violation could resolve this puzzle.

An international team of scientists has proposed a new method to search for the nEDM that promises to increase sensitivity by two orders of magnitude.[2] To measure a nEDM, polarized neutrons are placed in a weak magnetic field and strong electric field. The magnetic field causes neutron precession about the field direction with a predictable frequency. An EDM slightly modifies the frequency in proportion to the value and sign of the applied electric field. In the new method, a small quantity of another species, polarized helium-3, is placed in the same container as the neutrons. The helium-3 has a very similar magnetic dipole moment to the neutron but is known not to have an EDM greater than 10^{-29} $e \cdot$cm. The helium-3 precession occurs at nearly the same rate as the neutron precession, and any shift of the neutron frequency with respect to the helium-3 frequency that is proportional to the electric field will be the signature of an nEDM.

Both the neutrons and helium-3 are contained in a measurement cell filled with superfluid helium-4. Neutrons can

be bottled in a cell if their energy is low enough for them to be reflected by the Fermi potential of the walls; they are called ultracold neutrons (UCNs). UCNs are produced[3] in the cell by down scattering cold neutrons off the helium-4. The cross section for absorption of neutrons by helium-3 is highly spin-dependent, and the helium-3 serves as an analyzer of the relative precession frequency between the two species. If a neutron is absorbed, the reaction products lose their kinetic energy in the helium-4, which in turn scintillates. The detection of this scintillation light measures the beat frequency between the two species. As a control measurement, the precession frequency of the helium-3 is measured with superconducting quantum interference devices. The helium-3 is referred to as a comagnetometer because it occupies the same volume as the neutrons and measures the magnetic field.

The proposal has been reviewed by the Nuclear Science Advisory Committee and has been deemed to be the experiment with the greatest discovery potential for the new fundamental-neutron-science beam line at the Spallation Neutron Source.[4] The committee recommended a vigorous program of research and development (R&D) to validate the measurement technique and to work out the most significant engineering challenges

RESEARCH HIGHLIGHT
PHYSICS DIVISION

as well as eventual funding for the project. In order to control a variety of systematic errors that could produce a false result, the experimental apparatus must meet stringent design requirements. Significant progress has been made towards validation of the method.

The Electric Field

Whereas the sensitivity of the measurement is proportional to the magnitude of the electric field, this experiment has a goal of 50 kV·cm^{-1}, roughly five times that of previous measurements. Liquid helium-4 is a very good dielectric, i.e., will break down only at quite a high voltage. However, all previous measurements of its dielectric strength were performed with small surface areas and small gaps between the electrodes. The proposed experiment will have electrodes exceeding 600 cm^2 and a separation of 7.5 cm. We felt it necessary to demonstrate that we can achieve the desired voltage because the breakdown voltage is believed to scale as the square root of the separation.

A full-scale apparatus has been built at LANL to measure the dielectric strength in the relevant geometry. The electrodes are constructed so that the gap between them is variable. The high-voltage electrode is charged to about 50 kV with a power supply and then disconnected from the supply. As the electrode gap is increased, the voltage is multiplied to keep the field constant. Figure 1 shows a plot of the breakdown voltage as a function of separation. The curve in the figure is the breakdown voltage calculated assuming a square-root-of-the-gap dependence. The curve is normalized to the work of other investigators, all of which occurred below 10 mm. Our value of 570 ± 70 kV is the point at 73 mm. The voltage was stable for 11 h. In order to achieve 50 kV·cm^{-1} in the actual experiment, a larger variable capacitor will be attached in parallel with the fixed electrodes of the measurement cell.

The sign of the change in precession frequency with electric field for a real EDM should reverse if the sign of the field is reversed. Furthermore, at the very highest densities of UCNs, ionization produced by the decay or absorption of neutrons will discharge the electrodes slowly during the measurement. Thus, the value of the electric field needs to be known for both polarities. As part of our collaboration, Berkeley has proposed to use the Kerr effect to make an *in situ* measurement of the electric field. The Kerr effect is the rotation of polarized light passing through a high electric field. The size of the effect is proportional to the square of the electric field, and the proportionality constant is called the Kerr constant. Figure 2 shows the first measurement of the Kerr effect in superfluid liquid helium-4. The quadratic dependence is clear. The extracted value[5] of the Kerr constant is $(1.43 \pm 0.02^{(stat)} \pm 0.04^{(sys)}) \times 10^{-20}$ (cm/V)^2 at T = 1.5 K. The measurement at each voltage was made with roughly 3.5 cm of liquid helium-4 and took 1000 s. With a 50 cm path that is expected in the real application, the time for a measurement should be short enough to meet our needs.

The Magnetic Field

To preserve the polarization of the neutrons and the helium-3, magnetic-field uniformity must be 10^{-3}. The measurement cell must be shielded against μG external fields. The scheme

we have selected consists of a multilayer shield of highly permeable material that surrounds a superconducting shield. The constant field is produced by a *cos*θ coil inside the superconducting shield. The magnetic-field boundary conditions of the superconducing shield are incompatible with the coil. The coil will produce a very uniform field if it is wound inside an additional ferromagnetic layer. Because the experiment runs at cryogenic temperatures, it is necessary to select a ferromagnetic material that preserves its permeability at such temperatures. We have studied Metglas, a commercially available amorphous metal. Figure 3 shows the measured inductance of the Metglas as a function of temperature to be sufficient to meet our needs.

The Helium-3 Comagnetometer

The handling of the polarized helium-3 requires many complicated steps. We must

- produce highly polarized helium-3,
- inject it into a superfluid helium-4 bath while maintaining the polarization,
- maintain the polarization during the measurement, and
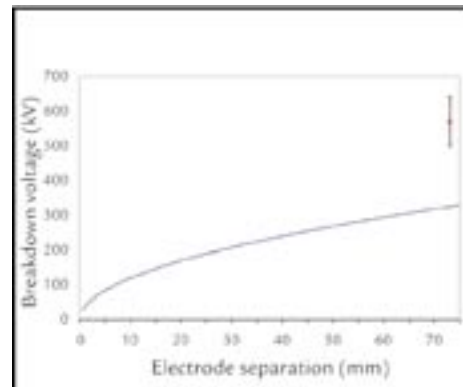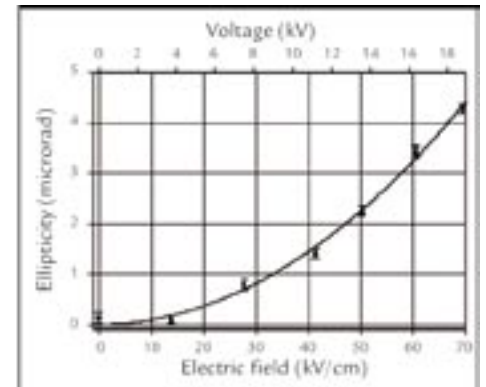- remove the helium-3 once it depolarizes.

Figure 2. The Kerr effect in liquid helium at T = 1.5 K: induced ellipticity as a function of the electric field between the electrodes. The potential difference between the electrodes is shown on the upper scale.

Figure 1. The breakdown voltage for liquid helium versus electrode separation.

The production step is accomplished with an atomic beam source. Helium-3 atoms at 1 K are injected into a quadrupole magnet. This magnet configuration produces a gradient field that is appropriate to focus only one spin through the apparatus. The other spin is removed with vacuum pumps. This type of device is known to produce very high polarization but sufficient intensity to meet our needs.

An atomic beam source has been built at LANL to verify its performance. In order to know the polarization, a second quadrupole magnet has also been built to act as an analyzer of the emitted atomic beam. The two magnets are separated by a region where radio frequency coils can manipulate the spins to measure the polarization. The polarization of the source has been measured to be $99.5 \pm 0.25\%$. The flux was approximately 4×10^{14} atoms/s.

The polarization must be maintained until the measuring cycle is complete. The problem has been broken into two parts, one where the atoms are injected into the system and one where the polarization is maintained in the measurement cell. The former is the subject of future R&D. The polarization relaxation time depends on the wall material of the container. The mechanisms for depolarizing the atoms vary significantly over the temperature range between 0.1–4.3 K. The expectation is that the relaxation time will decrease

as the temperature is lowered to 1 K and then rise rapidly below 1 K. The operating temperature of the experiment is 0.3 K. The cell walls have been chosen to be deuterated styrene impregnated with a deuterated wavelength shifter in order to minimize UCN absorption on the walls and to aid in the detection of the scintillation light.

Duke University is studying relaxation times at temperatures above 2 K. An ideal relaxation time is in excess of 8 h, which implies a depolarization of a few percent during an EDM measuring cycle. The Duke investigators are comparing the relaxation times in glass cells to those in cells where beads coated with deuterated styrene have been added. Thus far, they have achieved times in excess of 7 h in pure glass cells. They see no degradation when the coated beads are added.

The EDM collaboration has measured the diffusion coefficient for helium-3 in superfluid helium-4 between 0.45–0.95 K.[6] The measurement was carried out at Los Alamos Neutron Science Center employing neutron tomography. The results are shown in Figure 4. The measurement verifies predictions that the diffusion coefficient varies as T^{-7} below 0.7 K and allowed us to determine the temperature where the ballistic velocity of neutrons equals the diffusion velocity of the helium-3. Between 0.1–0.6 K, the average

velocity of the helium-3 is sufficient to allow escape from the superfluid helium-4. This realization leads towards the possible design of a system to remove depolarized helium-3 from a mixture by simply pumping on the bath.

The heat-wind technique can produce our initial charge of ultrapure helium-4 ($< 10^{-13}$ atoms of helium-3).[7] Phonons couple strongly to helium-3 and weakly to helium-4. The phonons can be used to blow the helium-3 away from a source of heat. When liquid helium-4 at $\sim$ 1 K is passed through a capillary tube surrounded by a resistive heater, only pure helium-4 passes. A cryostat designed for this purification process has been built at the Hahn-Meitner Institut and was operated at LANL. The first sample has been analyzed at Argonne National Laboratory and shown to have a purity of at least 10^{-12}.

Neutron Absorption Identification

The possibility to identify neutron absorption in liquid helium-4 has been reported by the method of after-pulses.[8] If the scintillation light produced by other mechanisms can be discriminated against, the scintillation signal has the possibility of being nearly background free, increasing the sensitivity of the measurement. The method of after-pulses consists of plotting the number of single photoelectrons detected in the 10 μs following the main scintillation pulse plotted versus the total scintillation light. The events due to absorption produce more highly ionizing particles than background beta particles. Both the highly ionizing particles and betas excite dimers in the helium-4, but the absorption events have a longer de-excitation time and thus, more late after pulses. Figure 5 shows the effect in data taken by the collaboration at the Hahn-Meitner Insitut. These data show the promise of greatly reducing a variety of backgrounds in the experiment.

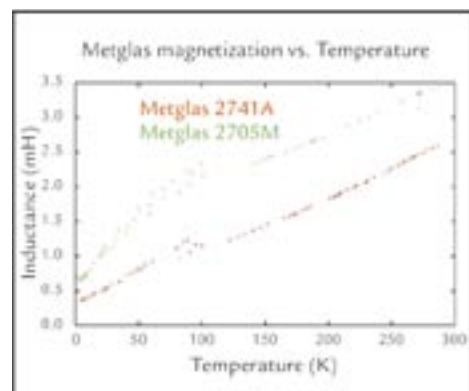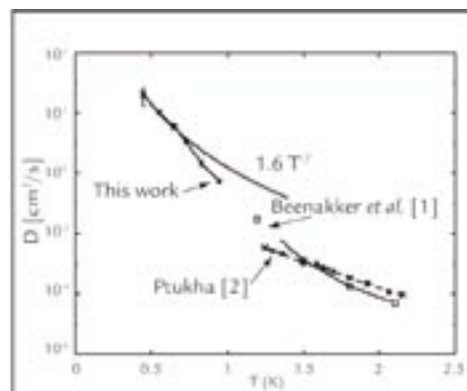*Figure 3. The inductance of Metglas versus temperature.*

Figure 4. A comparison of our results for the mass diffusion coefficient D of helium-3 in superfluid helium-4 below 1 K with those of previous workers at higher temperatures.
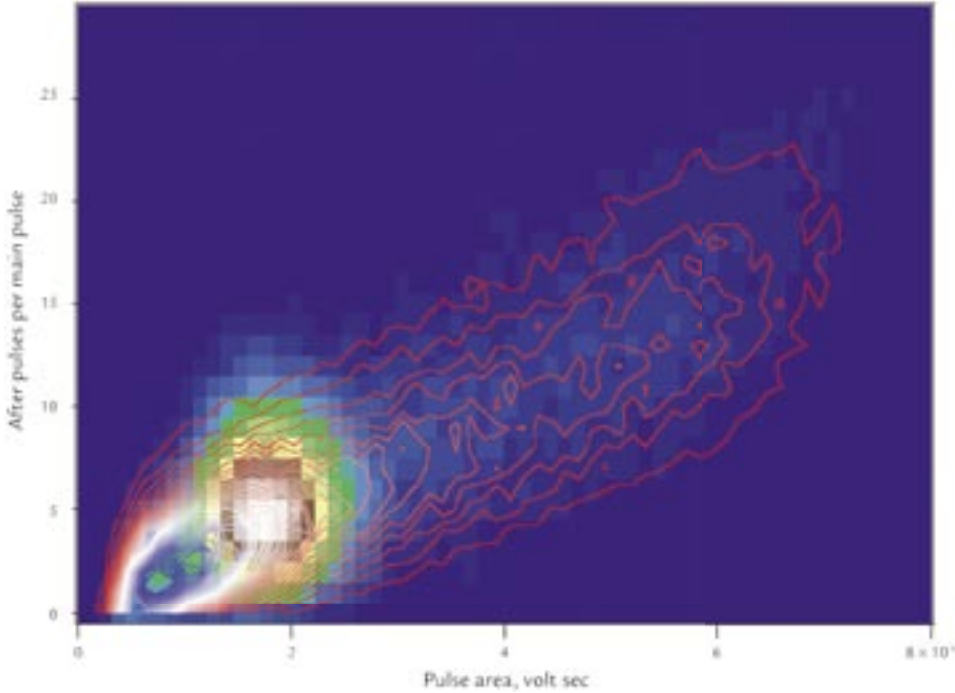
Figure 5. The separation between helium-3 absorption of neutrons and betas at 300 mK: number of after-pulses as a function of pulse height. The image plot is the absorptions and the contour plot is the betas.

Future R&D

A challenging task is to build a single piece of apparatus to contain all these different elements simultaneously that may be assembled and serviced. The engineering staff at LANL has made great progress toward reaching a reference design.

The EDM Collaboration has made great strides in developing a new experiment for a nEDM search. The collaboration has many other projects underway. Most of the crucial performance criteria of the detector components have been demonstrated. The future R&D is focused on bringing new concepts to the experiment to reduce backgrounds and systematic errors.

References

1. P.G. Harris *et al.,* "New experimental limit on the electric dipole moment of the neutron," *Physical Review Letters* **82**, 904–907 (1999).

2. R. Golub and S.K. Lamoreaux, "Neutron electric-dipole moment, ultracold neutrons and polarized ^{3}He," *Physics Reports* **237**, 1–62 (1994); M.D. Cooper *et al.,* "A new search for the neutron electric dipole moment," Los Alamos National Laboratory report LA-UR-02-2331 (April 2002).

3. E. Golub and J.M. Pendlebury, *Contemporary Physics* **13**, 519 (1972).

4. Report to NSAC, Subcommittee on Fundamental Physics with Neutrons (2003) 1.

5. A.O. Sushkov *et al.,* "Kerr effect in liquid helium at temperatures below the superfluid transition," *Physical Review Letters* **93**, 153003-1–153003-4 (2004).

6. S.K. Lamoreaux *et al.,* "Measurement of the ^{3}He mass coefficient in superfluid ^{4}He over the 0.45–0.95 K temperature range," *Europhysics Letters* **58**, 718–724 (2002).

7. P.V.E. McClintock, "An apparatus for preparing isotopically pure ^{4}He," *Cryogenics* **18**, 201–208 (1978).

8. K. Habricht, PhD Thesis, Technischen Universtat Berlin (1998).

Acknowledgment

For further information, contact Martin Cooper, 505-667-2929, mcooper@lanl.gov.

The Highest Energy Emission from Gamma-Ray Bursts

B.L. Dingus (P-23), M.M. González (P-23/University of Wisconsin), Y. Kaneko, R.D. Preece, M.S. Briggs (University of Alabama, Huntsville), C.D. Dermer (Naval Research Laboratory)

Astrophysical sources of gamma rays are the most extreme physical laboratories in the universe. Gamma rays, the highest-energy light, are produced by particles that are accelerated to relativistic energies. The highest-energy gamma rays are produced by the highest-energy particles and hence are excellent probes of these extreme environments.

Gamma-ray bursts top the list of extreme astrophysical sources. The release of energy in a gamma-ray burst exceeds that of a supernova. Almost all of that energy shows up from within a fraction of a second to a few minutes and emits almost entirely in gamma rays. It is likely that the formation of black holes produces gamma-ray bursts.

While gamma-ray bursts occur about once per day in the universe, they are very difficult to detect due to their short duration and unpredictable location. Special wide-field-of-view gamma-ray detectors must be used. These detectors must be above the Earth's atmosphere except for detecting gamma rays at the very highest energies, such as above about 0.1 TeV (Teraelectronvolt $= 10^{12}$ eV, which is about one trillion times the energy of visible-light photons).

Researchers in Neutron Science and Technology (P-23) have found a new high-energy feature in a gamma-ray burst that was detected by NASA's Compton Gamma-Ray Observatory. This feature points to interesting possible observations with Milagro, a high-energy detector located at LANL, which is operated by P-23 in collaboration with the University of Maryland, University of California -Irvine, -Santa Cruz, -Riverside, University of New Hampshire, New York University, Michigan State University, and George Mason University.

Producing the Highest-Energy Gamma Rays

The easiest way to produce light is by heat. For example, an incandescent light bulb heats up a filament, which then glows. On a larger scale, the light that is detected from the cosmic microwave background is due to the heat left over from the big bang. The wavelength of the light, which is another way of characterizing the energy of the photons, is related to the temperature of the source. A light bulb filament is 3000 K and produces visible photons, whereas the universe is 2.73 K and produces microwave photons. In order to produce gamma-ray photons, the temperature would have to be greater than 10^{13} K. Such high temperatures are unknown; in addition the distribution of gamma-ray energies is not consistent with such a thermal model.

Therefore, gamma rays require a more difficult mechanism to produce them. Charged relativistic particles are the key because they must emit gamma rays when they interact with magnetic fields, photons, or matter. These mechanisms are well studied with accelerators on Earth, such as the one at the Los Alamos Neutron Science Center. We can relate the energy of the gamma ray with the energy and type of the accelerated particle, the type of interaction, and the characteristics of the astrophysical medium. This description has many free parameters, so the more features we can observe, the better we can constrain the models of these sources. The features that we observe are the distribution of the energies of the gamma rays and how they vary with time. The maximum energy of the gamma rays detected is one of the easiest constraints to interpret. For example, the energy of the particle that produces the gamma ray must be larger than or approximately the same as the energy of the gamma ray for all types of these interactions.

Gamma-Ray Bursts

The origin of these powerful explosions is actively being debated. The duration is often as short as a few milliseconds and thus requires a very compact emission region. Also, the total energy released is so large that it exceeds the output of our sun during its entire lifetime. These characteristics have led researchers to believe that the astrophysical source must involve the creation of a black hole.

RESEARCH HIGHLIGHT
PHYSICS DIVISION

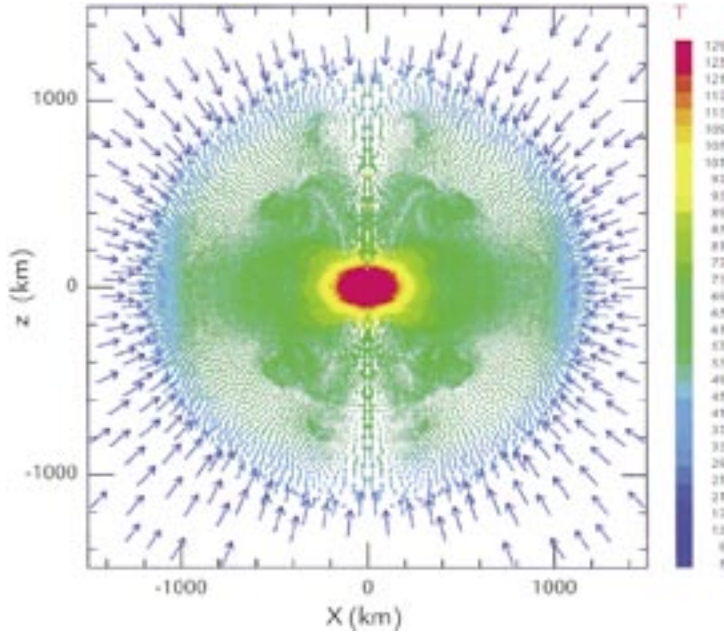# Nuclear Physics and Astrophysics Research Highlights

Figure 1. A computer simulation by Fryer, Woosley, and Heger of the collapse of a rotating massive star which is 1.5 s from forming a black hole. Color gives temperature in 10^9 K, and the arrows show the direction and magnitude of the particle velocity.

The details about how the birth of a black hole can cause a jet of relativistic particles to be accelerated involve fascinating but difficult physics. The conditions of such large gravitational and electromagnetic fields cannot be replicated on Earth. Researchers, such as Chris Fryer and Alex Heger of the Theoretical Astrophysics Group (T-6), are attempting to use computer simulations of the fundamental physics in this extreme environment to replicate these phenomena as shown in Figure 1.[1] These simulations cannot be exact due to the complexity of the problem and have yet to produce a complete understanding. These theories need more data from observations both in space and on the ground to provide constraints to the computer models.

Detecting Gamma Rays

Gamma rays are photons of light at an energy a few times 10^4 eV to greater than 10^{13} eV. This broad energy range requires different types of detectors. Below about 10^{11} eV gamma rays will not penetrate the Earth's atmosphere, so a space-based observatory is needed. NASA's Compton Gamma-Ray Observatory, shown in Figure 2, had four gamma-ray detectors covering different energy ranges with different fields of view.

Gamma rays cannot be focused onto small detectors as is done for visible photons with large mirrors. Instead, large detectors are required to cause the gamma rays to interact, turning their energy into ionizing radiation, which can be recorded.

Figure 2. Compton Gamma-Ray Observatory being deployed, as seen from the space shuttle. The four detectors, BATSE, OSSE (Oriented Scintillation Spectrometer Experiment), COMPTEL (Imaging Compton Telescope), and EGRET, are labled.
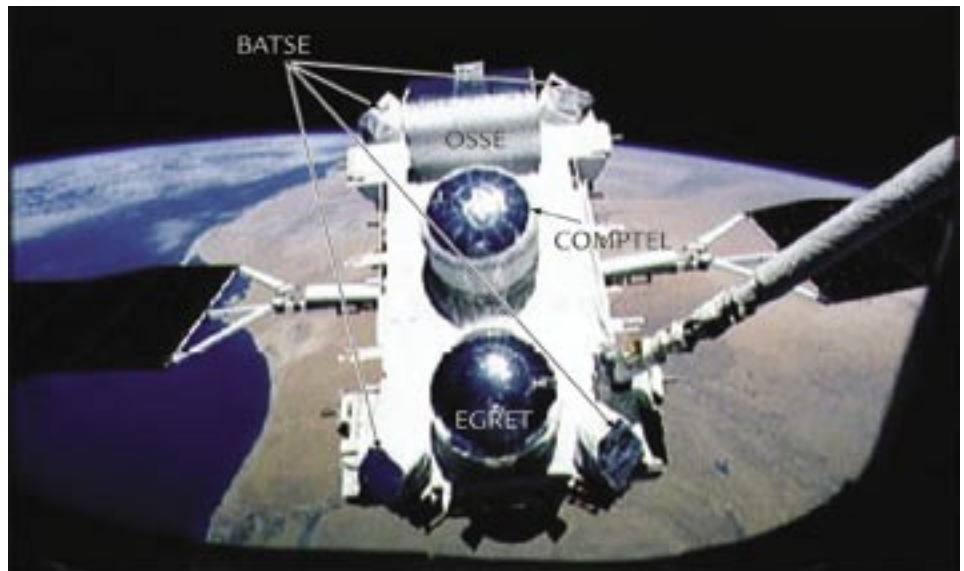
Astrophysical sources produce fewer high-energy gamma rays than low-energy gamma rays, thus larger detectors are required for higher-energy gamma rays. Due to the high cost of putting large detectors into space, the maximum energy of detectable gamma rays is limited. However, above 10^{11} eV, gamma rays produce showers of particles in the Earth's atmosphere that are detectable on the ground. Milagro, a gamma-ray observatory located at LANL, is the first large-field-of-view gamma-ray detector sensitive down to nearly 10^{11} eV. The large field of view is crucial to observing short duration, randomly and rarely occurring, gamma-ray bursts. An artist's conception of the shower of particles impacting Milagro is pictured in Figure 3.

A New Feature in the Highest-Energy Gamma Rays from Gamma-Ray Bursts

The largest-field-of-view detector on NASA's Compton Gamma-Ray Observatory was BATSE (Burst and Transient Source Experiment). BATSE was sensitive to gamma rays of a few times 10^4 eV up to a few times 10^6 eV, and detected nearly 3000 gamma-ray bursts during the nine years of this mission. EGRET (Energetic Gamma-Ray Experiment Telescope) was the detector on

the Compton Gamma-Ray Observatory that was sensitive to the highest-energy gamma rays, but detected only the brightest burst observed by BATSE.

Researchers in P-23 collaborated with researchers at the University of Alabama in Huntsville and the Naval Research Laboratory to combine data from BATSE and EGRET to examine the distribution of the energy of gamma rays, known as the energy spectrum, from the brightest gamma-ray bursts detected by BATSE. Twenty-six bursts were selected and one burst was found to have a new feature at the highest energies. Most gamma-ray burst spectra can be characterized as a single broad bump peaking in the center of the BATSE energy range. The peak of the bump typically evolves with time to lower energies as the brightness of the burst decays.

The energy spectrum of one burst, GRB941017, had an additional feature in the spectrum and produced up to the highest energies detectable as shown in Figure 4.[2] This feature decays slower than the typical broad bump, which is also detected in this burst. The total energy in this new feature exceeds that of the broad bump by at least a factor of two. The peak energy of this feature is beyond the range of the EGRET detection and suggests researchers may require a more powerful astrophysical source.

This observation raises many questions: What fraction of gamma-ray bursts has such high-energy emission? How high in energy does this feature extend? And most importantly, what type of interaction is creating this second feature? Due to the different temporal evolution of the broad bump and the high-energy feature, different types of particles may be responsible for the two types of emission. The lowest-energy broad bump is likely due to electrons interacting with magnetic fields, and the highest-energy feature could result from protons interacting with the gamma rays of the broad bump. However, in order for protons to produce gamma rays, the energy of the protons must be nearly as large as the highest-energy
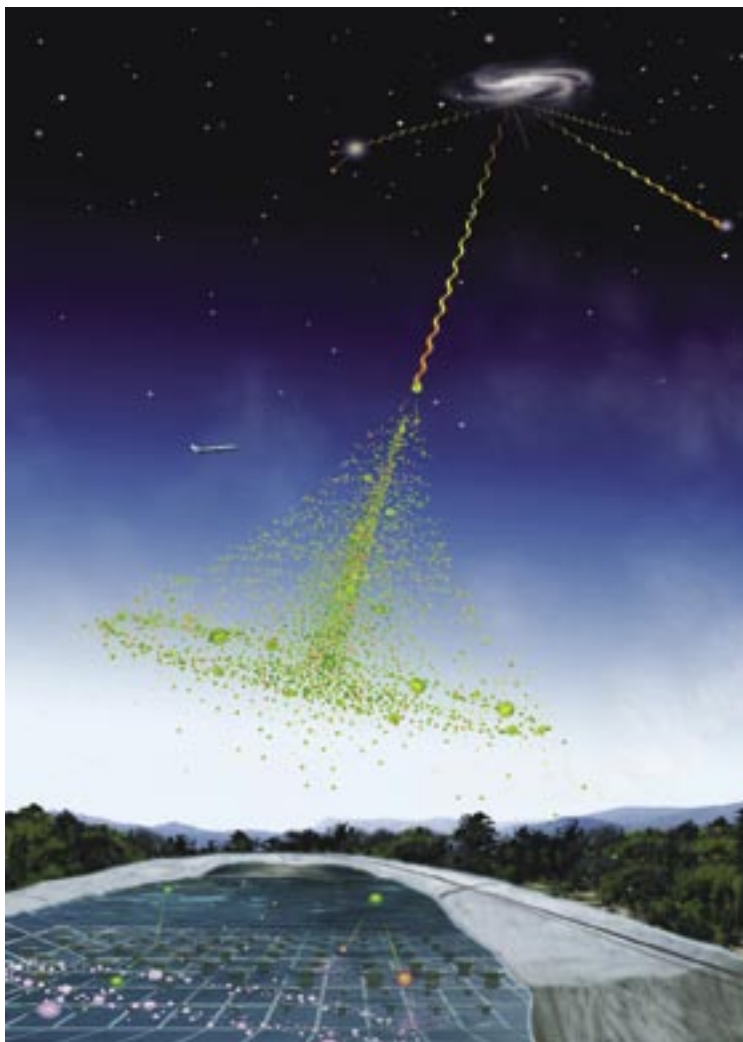

Figure 3. An artist conception of an air shower about to be detected by the Milagro gamma-ray observatory located in the Jemez Mountains.

particles known. These particles are known as ultra-high-energy cosmic rays. If this explanation for the high-energy feature of GRB941017 is confirmed by future observations, the long standing mystery of the origin of cosmic rays would be solved.

Future Observations

On November 20, 2004 NASA launched a new satellite, Swift, which is dedicated to detecting gamma-ray bursts. Swift will only detect gamma rays up to a few times 10^5 eV but will localize the direction and the distance to their origin very well. Milagro will look for evidence of $> 10^{11}$ eV gamma rays in coincidence

with Swift's detections of gamma-ray bursts. A prototype version of Milagro was operational during the time when BATSE was detecting gamma-ray bursts and found evidence for one gamma-ray burst which also had much more power released at higher energies than at the energies detected by BATSE.[3,4] Milagro is much more sensitive than this early prototype, and P-23 researchers are eagerly awaiting Swift's operation and more detections of the highest-energy gamma rays from gamma-ray bursts.
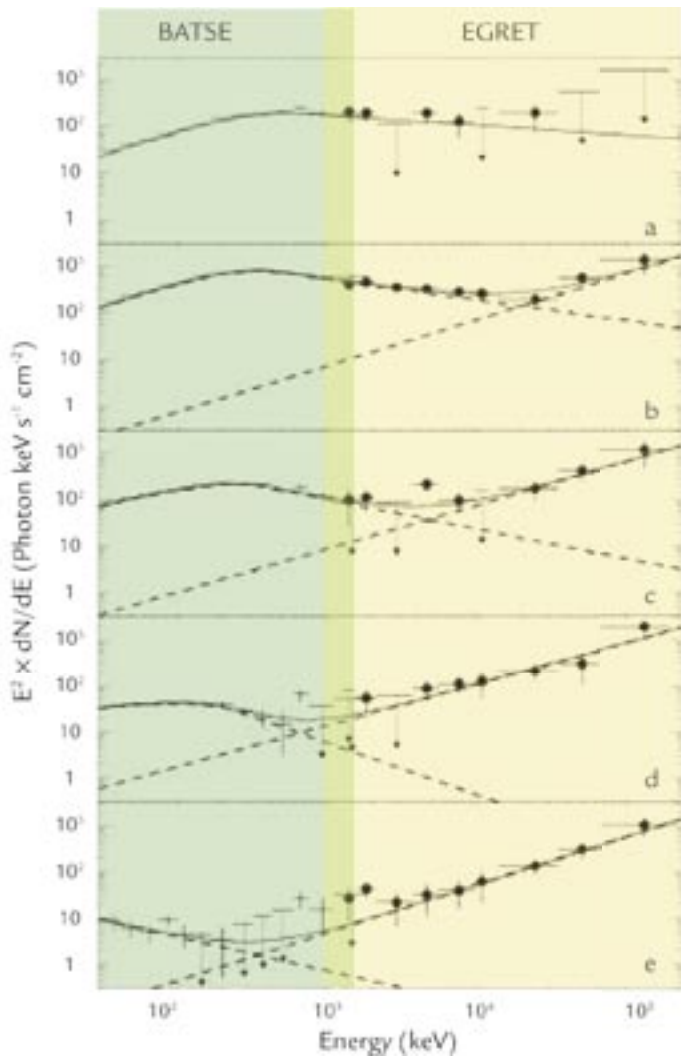
Nuclear Physics and Astrophysics Research Highlights

Figure 4. The energy spectrum from GRB941017 showing a new high-energy feature above 10^3 keV (= 10^6 eV). The five time intervals relative to the beginning of the burst were determined from the arbitary time intervals of spectra collected by EGRET and are (a) -18 to 14 sec, (b) 14 to 47 sec, (c) 47 to 80 sec, (d) 80 to 113 sec, and (e) 113 to 211 sec. (Reprinted from Nature Publishing Group.)

References

1. C.L. Fryer, S.E. Woosley, and A. Heger, "Pair-instability supernovae, gravity waves, and gamma-ray transients," *Astrophysical Journal* **550**, 372–382, 2001.

2. M.M. Gonzales *et al.,* "A γ-ray burst with a high-energy spectral component inconsistent with the synchrotron shock model," *Nature* **424**, 749–751, 2003.

3. R. Atkins *et al.,* "Evidence for TeV emission from GRB 970417a," *Astrophysical Journal*, **533**, L119–L122, 2000.

4. R. Atkins *et al.,* "The high-energy gamma-ray fluence and energy spectrum of GRB 970417a from observations with Milagrito," *Astrophysical Journal*, **583**, 824–832, 2003.

Muon Production with the PHENIX Muon Spectrometers and Color Glass Condensate

M.X. Liu, J.G. Boissevain, M.L. Brooks, P. Constantin, G.J. Kunde, D.M. Lee, M.J. Leitch, P.L. McGaughey, B. Norman, A.K. Purwar, W.E. Sondheim, H.W. van Hecke (P-25), J.P. Sullivan (ISR-1)

Understanding the substructure of nuclei is fundamentally important in nuclear physics. In modern theory, the strong nuclear interaction observed between nucleons (protons and neutrons) inside the nucleus is only a van-der-Waals-type residual force of a more fundamental interaction between the nucleon's constituents. This interaction involving quarks and gluons, collectively called partons, is referred to as quantum chromodynamics (QCD). Studying the parton distribution inside nuclei can shed light on why and how quarks and gluons are confined inside hadrons.

Our knowledge about parton distributions is mainly from deep inelastic lepton-nucleus scattering (DIS) experiments. In parton models, high-energy electron-nucleus scattering does not affect the nucleon as a whole, but just one of its constituents (Figure 1). Each constituent carries a fraction x of the nucleon's momentum with the probability density $f(x)$, also known as the parton density function (PDF).

In a naïve picture, the nucleus-parton distribution is simply the sum of the nucleon's PDFs inside the nucleus. However, the subject of this study is to see if internucleon interaction will eventually modify such distributions.

In a DIS scattering to the first order, an incoming lepton only couples with the charged quark or antiquark, not with a neutral-charged gluon. Using measured quark and antiquark distributions from DIS, one can calculate the gluon distribution employing QCD-based parton evolution equations. Figure 2 shows the gluon distribution inside the proton at a various probing energy scale represented as Q^2. It is interesting to note that the rapid rise in the small-x gluon PDF predicted by QCD calculation will eventually violate unitarity and lead to a breakdown in the parton model picture of scattering off independent partons. At a sufficiently high density, it becomes possible for a second gluon to overlap in space with the first, leading to gluon fusion, thus limiting the achievable gluon density at small-x. This saturation is sometimes described as the formation of a color glass condensate (CGC).[1]
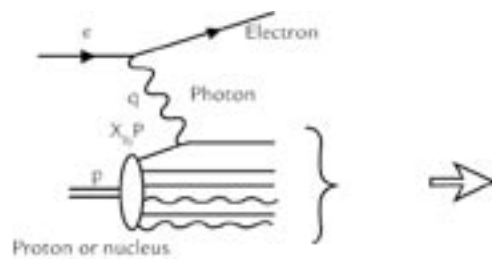

Figure 1. High-energy electron-nucleus interaction in the parton model. The incoming high-energy electron exchanges a virtual photon with a quark inside the nucleus. The collision probability is proportional to the quark density.
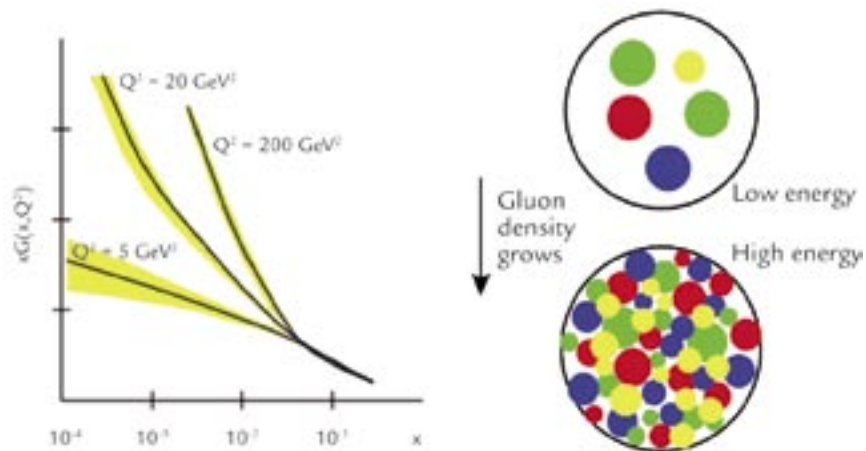

Figure 2. The gluon density $x*G(x, Q^2)$ grows rapidly as collision energy increases.
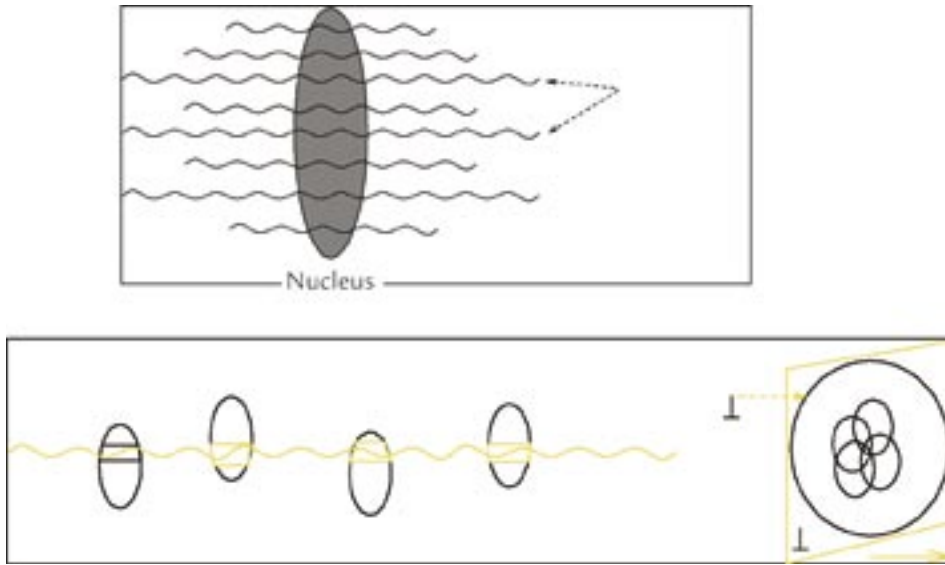
RESEARCH HIGHLIGHT
PHYSICS DIVISION

Figure 3. Small-x (or long-wavelength) gluons tend to overlap inside heavy nuclei and lead to gluon fusion.

One could expect that such saturation effects are particularly important for heavy nuclei where small-x gluons from different nucleons have a high probability to overlap in space (Figure 3).

The RHIC at BNL and the PHENIX Experiment

The Relativistic Heavy-Ion Collider (RHIC) at Brookhaven National Laboratory (BNL) collides two ion beams of various types, ranging from protons and deuterons to gold nuclei types, at energies of 100 GeV per nucleon. In such high-energy collisions, quarks and gluons interact directly, thus allowing us to directly probe the nucleus' parton distributions.

The PHENIX experiment at RHIC consists of a general-purpose detector that possesses unique attributes among the five RHIC experiments, including two spectrometers designed to measure high-energy muons over the forward and backward pseudorapidity range $1.2 < |\eta| < 2.4$. They are also the largest subsystems in the PHENIX experiment. The Subatomic Physics (P-25) PHENIX Team has led the design, construction, and operation of the muon spectrometers, and is now leading efforts to analyze the muon data. Figure 4

shows an artist's view of the PHENIX muon spectrometers.

PHENIX also has the ability to measure the centrality of individual ion-ion collisions, where centrality is a measure of the degree of overlap between the two colliding ions. One can compare particle production per nucleon-nucleon reaction in the head-on collisions with these in glancing ones. If there are no nuclear medium effects, i.e., the nucleus-parton distribution is simply the sum of the nucleons and there is no initial- and final-state interaction with nuclear medium, the particle yield per nucleon-nucleon collision will be independent of the collision's centrality.

Muon production in asymmetric deuteron-gold collisions at RHIC

In 2003, RHIC collided deuteron and gold nuclei at a center of mass energy of 200 GeV per nucleon pair. At this energy, most hadrons with a transverse momentum of Pt > 2 GeV arise from parton-parton interactions and can be used to probe the nuclear parton structure. Particle production in the deuteron direction (forward) is sensitive to small-x parton distribution in the gold nuclei, whereas particle production in the gold

direction (backward) is sensitive to the large-x parton distributions. It has been predicted that the gluon saturation at small-x in gold will suppress the particle production yield in the forward direction.[1] Very recently, other hadron-production mechanisms, such as quark recombination and coherent multiple-scattering models, could explain the observed suppression in the forward-rapidity region.[2]

The spectrometers were originally designed to measure muons, however, we recently developed new methods to expand the capability to include hadron measurement. In the following, we briefly discuss how to use muon spectrometers to measure hadrons in deuteron-gold collisions.

Due to the finite distance from the collision vertex to the hadron absorber in front of the muon tracking system, charged pions and kaons have a small probability to decay into a muon before the absorber, through decay modes such as $\pi \pm \rightarrow \mu \pm + \upsilon$, with the decay probability given by,

$$P_{decay} = 1 - e^{-\frac{L \cdot M}{\tau \cdot p}} \approx \frac{L \cdot M}{\tau \cdot p}$$

where L ~ 40 cm is the distance from the collision's vertex to the absorber and p, M, and τ are the momentum, mass, and proper lifetime of the particle. Collisions that occurred far from the absorber will have a higher probability to contain muons that originated from light meson decays than those that occurred close to the absorber. Figure 5 shows the normalized collision's vertex distribution for events with forward (positive z-direction) muons in deuteron-gold collisions. The large slope indicates a significant fraction of the muons are from pion and kaon decays.

In addition to muons from light meson decays, about 1% of hadrons from the collisions can also punch through the absorber and get into the muon spectrometer. These hadrons are identified by the muon identification (MuID) system. Most of the punch-through hadrons interact strongly and stop within

the first a few layers of the MuID absorbers while most muons will likely sail through all of the MuID absorbers.

Results

We studied the hadron production as a function of centrality and rapidity. Figure 6 shows the particle yield ratios per nucleon-nucleon collisions versus rapidity of the most central collisions (0%–20%) to peripheral collisions (60%–88%). Without nuclear medium effects, this ratio should be unity.

We observed suppression in charged hadron yield at forward rapidity and enhancement at backward rapidity in the ratio between central and peripheral deuteron-gold collisions. The forward suppression is consistent with the expectation of gluon shadowing or saturation in the small-x region in large nuclei. For a typical hadron of transverse momentum Pt ~ 1.5 GeV, the x-value probed in gold nuclei at the very forward rapidity $y \approx -2$ is estimated to be 2×10^{-3}, and at the very backward direction $y \approx -2$, the x-value is close to 1×10^{-1}. Further detailed comparisons with various theoretical approaches are necessary in order to discriminate between different models, such as CGC and parton recombination models. Currently, we have no sound theoretical understanding for the enhancement in the backward rapidity. Antishadowing (enhancement) in parton distribution at large-x or final-state multiple scattering could lead to such effects.
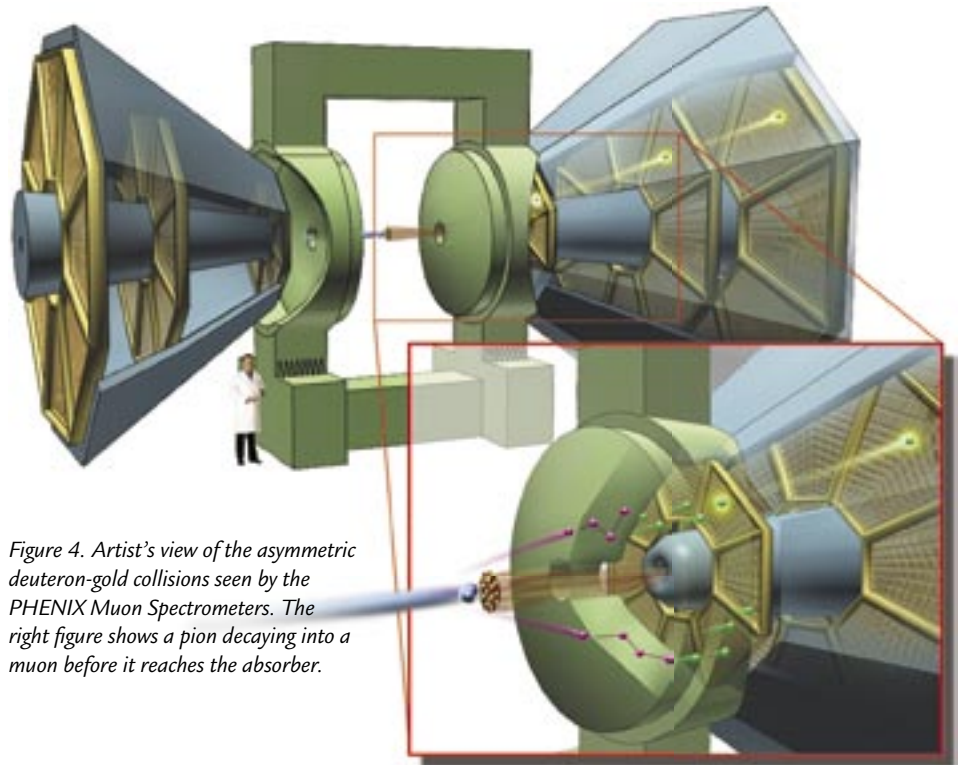

Figure 4. Artist's view of the asymmetric deuteron-gold collisions seen by the PHENIX Muon Spectrometers. The right figure shows a pion decaying into a muon before it reaches the absorber.
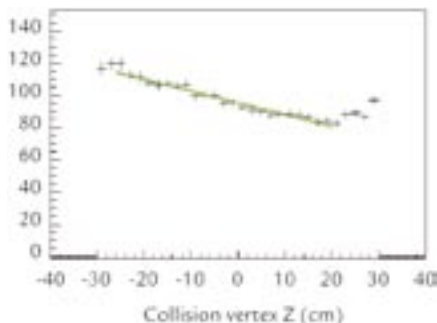

Figure 5. Normalized collision vertex distribution for muon events. The slope indicates that a significant fraction of muons is from pion and kaon decays.
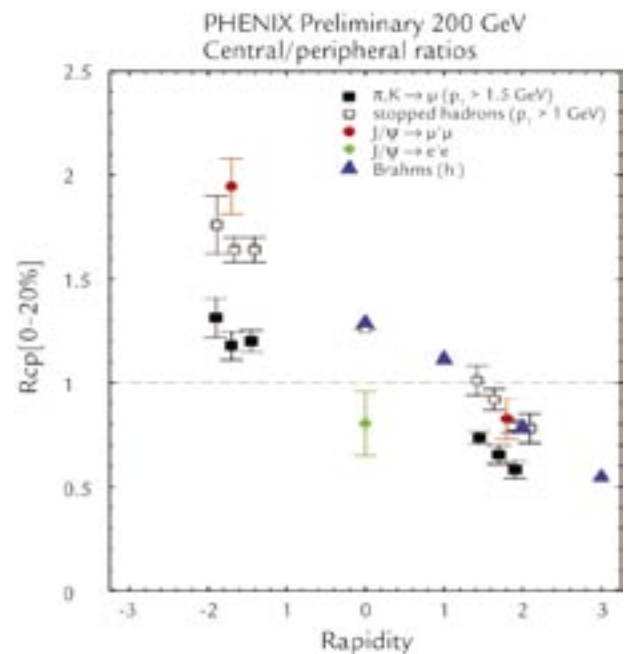

Figure 6. The ratio of particle yield per nucleon-nucleon reaction in the very central deuteron-gold collisions relative to the peripheral one.

Conclusion

We have studied high-energy particle production at the forward and backward directions in asymmetric deuteron-gold collisions at RHIC. The preliminary results are consistent with parton shadowing or CGC saturation models at small-x, and antishadowing or Cronin effects at large-x inside gold nuclei. In the near future, we expect to measure heavy flavor production in a similar kinematic region. Such measurements are particularly important since the final-state multiple scattering effect is expected to be minimal for heavy quarks, thus they could provide an unambiguous experimental test of various particle production models.

References:

1. L.D. McLerran and R. Venugopalan, "Computing quark and gluon distribution functions for very large nuclei," *Physical Review D* **49**, 2233–2241 (1994).

2. R. Hwa, C.B. Yang, and R.J. Fries, "Hadron production in the forward and backward rapidities in dAu collisions at RHIC," e-Print Archive preprint nucl-th/0410111, (13 Apr 04);
J. Qiu and I. Vitev, "Coherent QCD multiple scattering in proton-nucleus collisions," e-Print Archive preprint hep-ph/0405068, (7 May 04).

3. M.X. Liu (PHENIX Collaboration) Talk at Quark Matter 2004 Conference, Oakland, CA, Jan. 2004; D. d'Enterria, "Hard spectra and QCD matter: experimental review," e-Print Archive preprint nucl-ex/0403047, (2 Jun 04);
R.G. de Cassagnac, Talk at Quark Matter 2004 Conference, Oakland, CA, Jan. 2004; R.G. de Cassagnac, "J/ψ production and nuclear effects for d + Au and p + p collisions in PHENIX, e-Print Archive preprint nucl-ex/0403030, (16 Mar 04).

Acknowledgment

The World's Greatest Science Protecting America

http://www.lanl.gov/physics

J/ψ and Charm Quark Production Measurements with the PHENIX Detector at RHIC

P.L. McGaughey, J.G. Boissevain,
M.L. Brooks, G.J. Kunde, D.M. Lee,
M.J. Leitch, M.X. Liu, B. Norman,
W.E. Sondheim, H.W. van Hecke (P-25),
J.P. Sullivan (ISR-1)

The Relativistic Heavy-Ion Collider (RHIC) facility at Brookhaven National Laboratory was designed to collide counter-rotating beams of gold atoms with velocities near the speed of light. When two gold atoms suffer a head-on collision at these high speeds, it is expected that a new phase of matter may be formed. This new type of matter, called the quark-gluon plasma (QGP), consists of quarks and gluons that are no longer bound inside the protons and neutrons contained in the gold atoms. Plasma formation can be understood by an analogy to boiling water. As liquid water heats, it begins to boil, evaporating to form a gas. Likewise, protons and neutrons heat up and begin to evaporate quarks and gluons.

Figure 1. The PHENIX detector during construction. The central magnet is in the middle. The two muon magnets are the lampshade-shaped objects on the left and right.

The PHENIX Experiment and QGP Formation

The PHENIX experiment[1] at RHIC is designed to search for signatures of QGP formation. Matsui and Satz[2] have proposed that the J/ψ particle, which consists of a charm and anticharm quark bound together, is not formed in the presence of a QGP. Due to the relatively large size of the J/ψ, the attractive force between the two charm quarks can be greatly reduced by interference with the strong fields associated with the light quarks and gluons liberated in the plasma. This behavior is analogous to the Debye screening process in chemical solutions and atomic plasmas. The result is that the two charm quarks are unlikely to form a bound state. Instead, they combine individually with light quarks to form a pair of D mesons. Therefore, an

experimental signature of QGP formation is the observation of a strong suppression of J/ψ production in central gold-gold collisions, relative to peripheral collisions. An increase in D meson production is also expected. However, because the total yield of D mesons is much larger than for the J/ψ, the latter effect will probably be too small to observe.

In order to quantify J/ψ suppression in the QGP, it is critical to understand J/ψ production in collisions where the QGP is not formed. Examples of these

are proton-proton and proton-gold collisions at similar energies. At RHIC energies, the production of charm quarks is dominated by the gluon fusion process $g + g \rightarrow c + \bar{c}$. Thus, charm production is sensitive to the gluonic content of the colliding nuclei. It's also known that J/ψ production is somewhat suppressed by the ordinary nuclear medium, relative to the proton, and that the level of suppression is dependent upon the momentum vector of the J/ψ. These nuclear effects have been characterized as initial-state effects, which refer to the modification of J/ψ formation

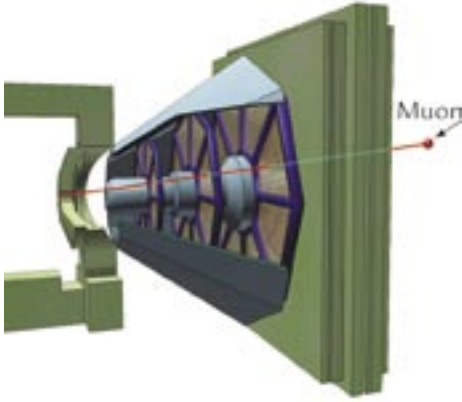# RESEARCH HIGHLIGHT

PHYSICS DIVISION

Figure 2. A schematic drawing of one muon arm, with the muon magnet and tracking chambers shown in blue. On the right is the muon identifier. A typical muon trajectory is drawn in red, traversing the arm from left to right.

in a nucleus, and final-state effects relevant to the propagation of the J/ψ through the nucleus. Initial-state effects can arise from changes in the gluon momentum distributions in a nucleus. Final-state effects include multiple scattering, energy loss, and dissociation of the J/ψ. It's important to measure open charm (D mesons) to help separate initial- from final-state effects, because D mesons suffer different final-state effects than the J/ψ.

The PHENIX experiment, shown under construction in Figure 1, consists of two central arms and two muon arms. Each muon arm consists of a tracking system, which measures the momentum vector of each muon, together with a muon identifier, which separates muons from other particles and provides the muon trigger for PHENIX. Our team led the design, construction, and operation of the muon tracking system over a period of more than ten years. Staff from Oak Ridge National Laboratory led the muon identification system effort. We also pioneered the use of cathode-strip-chamber technology for the high-precision tracking chambers used to accurately measure the muon trajectories and momentum. The muon arms measure the decay $J/\psi \rightarrow \mu^+\mu^-$ over the rapidity range of $1.2 < |\eta| < 2.4$, while D mesons are detected via the semileptonic decay $D \rightarrow \mu + X$.

A schematic of the operation of a muon arm is given in Figure 2. A muon originating from the intersection point of the two gold beams (left side of drawing) travels through the steel of the central magnet into the muon lampshade magnet. Particles other than muons generally interact in the steel and are stopped there. Three stations of cathode strip chambers (vertical blue bars on the drawing) inside the magnet accurately measure the trajectory of each muon. Due to the presence of a large magnetic field inside the magnet, a muon follows a curved trajectory. By measuring this curvature, we determine both the muon's charge and momentum. After exiting the muon magnet, the muon encounters alternating layers of steel and Iarocci tube detectors in the muon identifier, which remove any remaining backgrounds due to particles other than muons. The depth of penetration is a rough measure of the muon's energy, which we use to provide a trigger to PHENIX, requesting that the data for this beam crossing be recorded.

Experimental Results

PHENIX has recently measured proton-proton, deuterium-gold[3], and gold-gold collisions at energies of 100 GeV per nucleon. Preliminary results for the J/ψ differential cross section versus rapidity from proton-proton collisions are shown in Figure 3. The shape of differential cross section is consistent with predictions of perturbative quantum chromodynamics (QCD), based upon gluon fusion diagrams. The total cross section times branching ratio is 159 nb ± 8.5% (fit uncertainty) ± 12.3% (systematic uncertainty). These proton-proton J/ψ data serve as the baseline for extracting nuclear effects from the deuterium-gold data.

The ratio between the deuterium-gold and proton-proton J/ψ data versus rapidity is given in Figure 4. While the ratio is near one at backward (negative) rapidity, a significant suppression is observed at forward (positive) rapidity. The latter region corresponds to low-Bjorken-x (fraction of the proton momentum) values

for the gluons in deuterium, where we expect the gluons to be suppressed, due to the presence of the color glass condensate[4] or as a result of other models of gluon shadowing. Also shown in Figure 4 are theoretical predictions of shadowing from Vogt[5] and Kopeliovich[6]. The data favor less shadowing than in the Kopeliovich model, but the uncertainties are large.

Also of interest are the transverse momentum distributions of the J/ψ. The data are consistent with nuclear suppression at low pT and enhancement at high pT, similar to that seen previously by E866.[7] This behavior, which is often referred to as the Cronin effect[8], comes about from the multiple scattering of particles as they propagate through a nucleus, leading to an average increase in their transverse momentum.

PHENIX has the ability to measure the centrality of individual ion-ion collisions, where centrality is a measure of the degree of overlap of the two ions. Using the beam-beam Cerenkov counters located at small angles with respect to the two ion beams, the yield of produced particles is determined, which is directly correlated with the collision centrality. The centrality dependence of the J/ψ yield can then be computed. Shadowing of the gluons in gold is again observed, consistent with theory, with little centrality dependence. However, a strong increase with centrality is observed for the yield of J/ψ produced at backward rapidity, which is inconsistent with theory.

Open charm particles (D mesons) have been measured by both the PHENIX[9] and the STAR[10] experiments at central rapidity. Data is available from proton-proton and deuteron-gold collisions. Both experiments report total cross sections in reasonable agreement with predictions of perturbative QCD. The deuteron-gold data show no strong nuclear dependence, which is not surprising as these data do not correspond to the shadowing region and have poor statistics at high pT. Open charm data from the muon arms are presently under analysis and will be able to address both the shadowing and high-pT regions.

Data from gold-gold collisions is presently under intense study. Due to the large number of particle tracks in each muon spectrometer, track reconstruction is much more difficult than for the lighter ions. After we made significant upgrades to the reconstruction software, we are now able to reliably detect J/ψ particles in peripheral collisions. Figure 5 shows dimuon mass plots from each arm. The peaks with mass near 3.1 GeV correspond to the J/ψ. Further study of these data is required to determine and optimize the reconstruction efficiency versus centrality.

Conclusion

The PHENIX muon arm physics program is well underway after more than 10 years of design, construction, and installation. Both muon arms are completely functional and working within design specifications. The first measurements of J/ψ production in proton-proton and deuteron-gold collisions at RHIC energies have been presented and are providing important insight into the nature of gluon shadowing and the Cronin effect. An excellent set of data from gold-gold collisions has been recorded and the analysis is well underway. Within the near future, we should be able to determine if the J/ψ signal is suppressed enough in these collisions to indicate the formation of a quark-gluon plasma.

Figure 3. Rapidity distribution for J/ψ produced in proton-proton collisions at 200 GeV. The red points are from Run 3, which has the highest integrated luminosity to date.
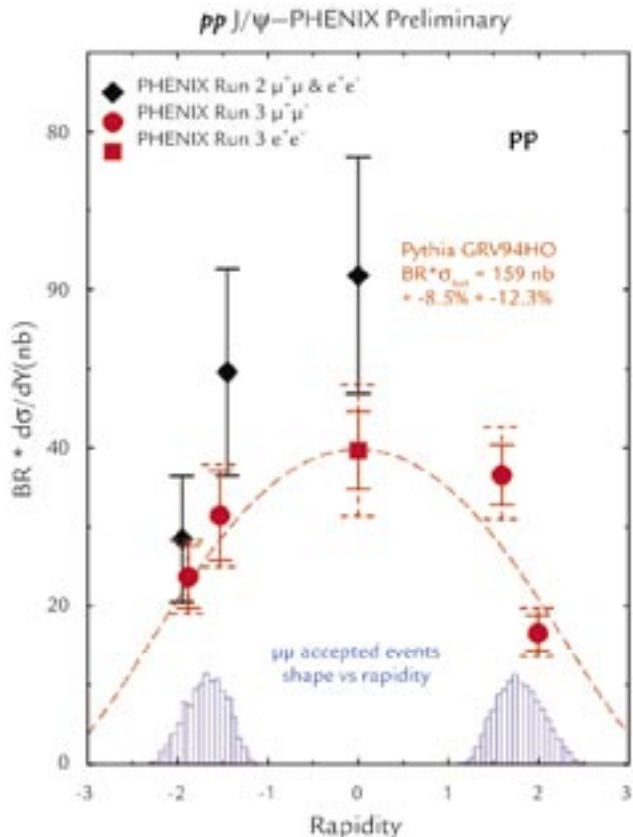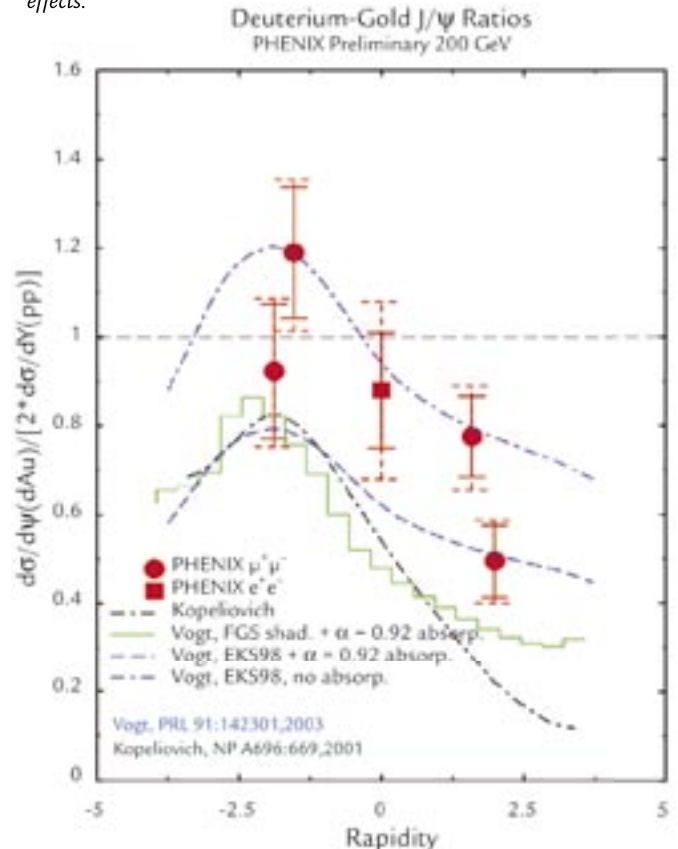

Figure 4. The ratio of J/ψ cross sections from deuteron-gold and proton-proton collisions. The data at positive rapidity correspond to the shadowing region. The colored curves are various theoretical predictions of nuclear effects.
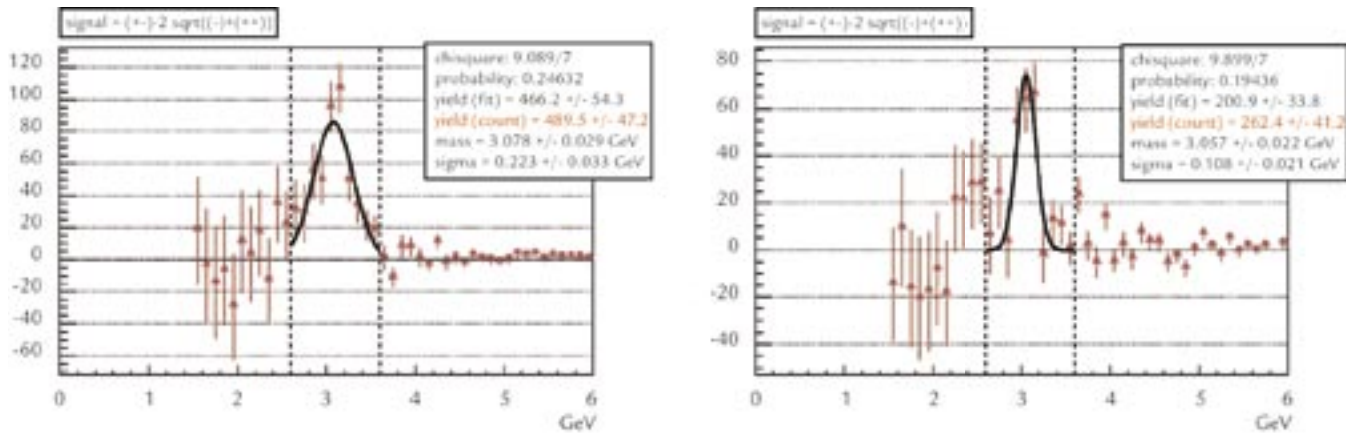
Figure 5. Preliminary dimuon mass distributions from peripheral gold-gold collisions after background subtraction. The left plot is for the south muon arm, while the right plot is for north. The peak corresponds to the J/ψ particle.

References

1. A web-based introduction to the PHENIX Experiment is located at: http://www.phenix.bnl.gov/phenix/WWW/intro/.

2. T. Matsui and H. Satz, "J/ψ suppression by quark-gluon plasma formation," *Physics Letters B* **178**, 416–422 (1986).

3. R.G. de Cassagnac, "J/ψ production and nuclear effects for d+Au and p+p collisions in PHENIX," *Journal of Physics G* **30**, S1342–S1345 (2004).

4. L. McLerran, "The quark gluon plasma and the color class condensate: 4 lectures," *RHIC Physics Lectures,* e-Print Archive: hep-ph/0311028 (2003).

5. S.R. Klein and R. Vogt, "Inhomogeneous shadowing effects on J/ψ production in *d*A collisions," *Physical Review Letters* **91**, 142301-1–142301-4 (2003).

6. B. Kopeliovich, A. Tarasov, and J. Hüfner, "Coherence phenomena in charmonium production off nuclei at the energies of RHIC and LHC from pQCD, saturation and hydrodynamics," *Nuclear Physics A* **696**, 669–714 (2001).

7. E866/NuSea Collaboration, "Measurement of differences between J/ψ and ψ′ supression in *p-A* collisions at 800-GeV/c," *Physical Review Letters* **84**, 3256–3260 (2000).

8. J.W. Cronin, *et al.,* "Production of hadrons with large transverse momentum at 200-, 300-, and 400-GeV," *Physical Review D* **11**, 3105–3123 (1975).

9. S. Kelly, "The PHENIX measurement of heavy flavor via single electrons in p-p, d-Au, and Au-Au collisions at $\sqrt{S_{NN}}$ = 200 GeV," *Journal of Physics G* **30**, S1189–S1192 (2004).

10. A. Tai, "Measurement of open charm production in d+Au collisions at $\sqrt{S_{NN}}$ = 200-GeV," *Journal of Physics G* **30** S809–818 (2004); L. Ruan, "Open charm yields in 200-GeV p+p and d+Au collisions at RHIC," *Journal of Physics G* **30**, S1197–S1200 (2004).

The NPDGamma Experiment

J.D. Bowman, M. Gericke, G.S. Mitchell, S.I. Penttila, G. Peralta, P.-N. Seo,
W.S. Wilburn (P-23) representing the NPDGamma Collaboration.

The nature of weak interactions between strongly interacting hadrons is not well understood. The NPDGamma ($\bar{n} + p \rightarrow d + \gamma$) experiment[1] currently being commissioned at the Los Alamos Neutron Science Center (LANSCE), will study the parity-violating weak interaction between the most common hadrons: protons and neutrons. The hadronic weak interaction is observed in nuclei and nuclear processes[2], but interpretation of these experiments is difficult because of the complicated many-body dynamics of a nucleus. The goal of the NPDGamma experiment is to measure the parity-violating directional gamma-ray asymmetry in the reaction ($\bar{n} + p \rightarrow d + \gamma$) to an accuracy of 5×10^{-9}, which is approximately 10% of its predicted value.[3,4] Such a result, in a simple system, will provide a theoretically clean measurement of the weak pion-nucleon coupling, thus resolving a long-standing question in nuclear physics.

In early 2004, all elements of the NPDGamma experiment were successfully commissioned, with the exception of the liquid-hydrogen target. Following final construction of the target and verification of appropriate safety measures for its operation, it will be installed and commissioned in summer 2005. This will allow the experiment to begin taking production data.

Theory Background

The flavor-conserving weak interaction between hadrons is the most poorly tested aspect of electroweak theory.[4] While much is known about quark-quark weak interactions at high energies, the low-energy weak interactions of hadrons (particles made of quarks, such as the nucleons—the proton and the neutron) are not well measured. At low energies, the effects of the weak interaction are typically obscured by other processes, making their experimental study challenging. The weak nucleon-nucleon interaction has been expressed in various forms and models.[3,4,5] Regardless of the formalism, pion exchange is particularly interesting because it is the longest-range component of the interaction, and is therefore presumably the most reliably calculable. The hadronic exchange of neutral currents, which is expected to dominate the weak pion exchange between nucleons, has not been isolated experimentally in an unambiguous way. For both of these reasons, the coupling constant H_π^1 for pion exchange in the weak nucleon-nucleon interaction is of special interest.

An accurate measurement of H_π^1 in a simple nucleon-nucleon system is needed to resolve previous experimental inconsistencies. A two-nucleon system such as in the $\bar{n} + p \rightarrow d + \gamma$ process is sufficiently simple that the measured asymmetry of the emitted gamma rays can be related to the weak meson-nucleon-nucleon coupling with negligible uncertainty to nuclear structure. The relationship between the parity-violating asymmetry A_γ and H_π^1, where A_γ is the correlation between the direction of emission of the gamma ray and the neutron polarization, is calculated to be $A_\gamma \approx -0.045\, H_\pi^1$. The goal of NPDGamma is to measure A_γ to a precision of $\pm 5 \times 10^{-9}$, which will determine H_π^1 to $\pm 1 \times 10^{-7}$. Such a result will clearly distinguish between the values for H_π^1 extracted from experiments in nuclear systems as well as between predictions by various theories of the weak interaction of hadrons in the nonperturbative quantum chromodynamics regime.
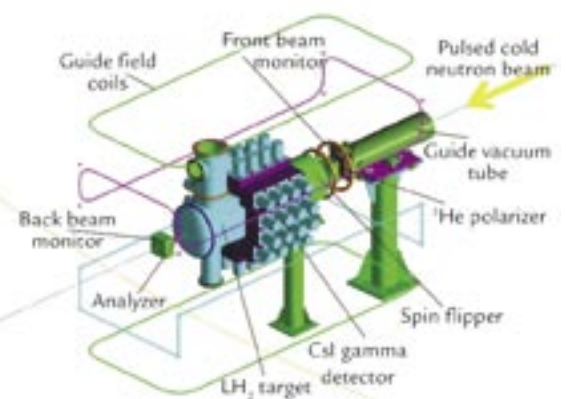

Figure 1. A drawing of the NPDGamma apparatus.

RESEARCH HIGHLIGHT
PHYSICS DIVISION

Figure 2. Photo of the FP12 chopper, before it is covered with concrete shielding. The horizontal yellow structure contains the neutron guide, and the aluminum housing in the center contains the spinning chopper element. A gap in the chopper allows neutrons of the desired energy range to pass, while the lower-energy neutrons are absorbed in the chopper coating of gadolinium oxide.

Experiment

To determine H_π^1 with an uncertainty of 1×10^{-7}, we must achieve a statistical uncertainty of 0.5×10^{-8} on A_γ. This means that the experiment must detect a few $\times 10^{17}$ of the 2.2 MeV gamma rays from the $\bar{n} + p \rightarrow d + \gamma$ reaction. In addition, possible systematic errors in the experiment require careful attention. The tiny parity-violating signal in the reaction will be isolated by flipping the neutron spin. The real asymmetry will change sign under spin reversal, while spin-independent false asymmetries will not. The weak interaction is the only fundamental particle interaction that can produce a parity-violating signal; parity violation is simply described as a difference between a physical process and its mirror image. For example, in the $\bar{n} + p \rightarrow d + \gamma$ reaction, if more gamma rays are emitted in the same direction as the neutron spin, rather than in the opposite direction, then that is a parity-violating signal and must be caused by the weak interaction. The experiment then consists of observing the direction of emission of the gamma rays from many $\bar{n} + p \rightarrow d + \gamma$ captures, and if there is an asymmetry in their distribution with respect to the neutron polarization direction, the effect of H_π^1 has been observed.

The requirements for the experiment are the following: a large number of polarized, cold neutrons; a method of flipping the neutron polarization; a proton target; and a detector system for the 2.2 MeV gamma rays.

The experiment consists of a pulsed, cold neutron beam, transversely polarized by transmission through polarized helium-3, with polarization reversal achieved on a pulse-by-pulse basis by a radio frequency spin flipper (RFSF). The neutrons are incident on a liquid para-hydrogen target. The 2.2 MeV gamma rays from the capture reaction will be detected by an array of cesium iodide scintillators coupled to vacuum photodiodes and operated in current mode. A drawing of the setup for the experiment is shown in Figure 1.

Cold Neutron Beam and Polarizer

The experiment requires a high flux of cold neutrons, with energies below 15 meV. While such neutrons are available from cold moderators at both reactors and spallation neutron sources, the nature of the neutron flux from a pulsed spallation source provides a very powerful diagnostic tool for a number of possible systematic effects for this experiment. At LANSCE, the cold neutron source consists of a liquid-hydrogen moderator coupled to the 20 Hz pulsed neutron source. At cold-neutron energies, it is possible to use neutron guides to transport neutrons. The neutron guide possesses a reflectivity that is close to unity for neutrons incident at glancing angles below a (well-known) critical angle, and the reflectivity falls sharply above this angle. The function of the neutron guide is to conserve the high-cold-neutron flux available near the moderator.

For the experiment, a new beam line and neutron guide, Flight Path 12 (FP12), have been built at the Lujan Neutron Scattering Center.[6] One element of this beam line is a frame overlap chopper, a large rotating disk coated with gadolinium oxide. A photo of the chopper before it was covered with shielding is shown in Figure 2. The purpose of the chopper is to keep each pulse's slowest neutrons from being passed by the faster neutrons from the following pulse. The chopper was commissioned in early 2004 and its effect is shown in Figure 3. The chopper is a key element of the flight path because it allows us to unambiguously associate a neutron's time of flight with its energy.

In order to observe parity violation (in the distribution of gamma rays with respect to the neutron polarization direction), the experiment requires polarized neutrons. Cold neutron beams can be polarized in several ways, but the best technology for NPDGamma is a helium-3 spin filter. Helium-3 spin filters are compact, possess a large phase-space acceptance, and produce a negligible fraction of gamma-ray background. In addition, they
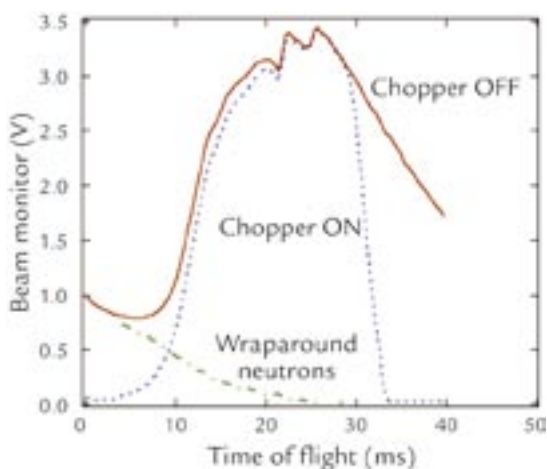

Figure 3. A plot showing beam-monitor response versus neutron time of flight. The beam-monitor voltage is proportional to the number of neutrons passing through it, and the time of flight is a measure of the neutron energy. The general shape of the red and blue curves (peaked in the middle) is characteristic of the neutron-energy spectrum. The chopper function is evident in the difference between the red and blue waveforms (shown as the green curve at low time of flight, or high energy) where the chopper eliminates low-energy neutrons from lingering until the succeeding beam pulse.

do not require strong magnetic fields or produce field gradients. This is important for the control of systematic errors in the experiment. The thickness of the spin filter can be optimized for polarization versus transmission.

Neutron Spin Flipper

For NPDGamma the neutron spins are flipped on a 20 Hz pulse-by-pulse basis with a RFSF. The RFSF is a shielded solenoid that operates according to the well-known principles of nuclear magnetic resonance. In the presence of a homogeneous constant magnetic field and an oscillating magnetic field in a perpendicular direction, the neutron spin will precess, and the amplitude of the oscillating field can be selected to precess the spin by 180° as the neutron travels through the spin-flipper volume. The spin flip is introduced on a pulse-by-pulse basis by simply turning the radio frequency field on and off. The solenoid produces only negligible external magnetic fields and field gradients, an important property given the possible sensitivity of the detector apparatus to magnetic-field-induced gain shifts. The spin-flipper efficiency was measured in commissioning data in early 2004 and determined to be 95% ± 5% over the extent of the neutron beam.

Proton Target

In the liquid-hydrogen (proton) target, it is essential that the polarized neutrons retain their polarization until they capture. Many of the neutrons will scatter in the target before they are captured, and the spin dependence of the scattering is therefore important. The ground state of the hydrogen molecule (known as para-hydrogen) has spin of zero *(J=L=S=0),* and the first excited state, the lowest ortho-hydrogen state, is at 15 meV above the para- state. A large fraction of the cold neutrons possess energies lower than 15 meV. Because these neutrons cannot excite the para-hydrogen molecule into its first excited state, only elastic scattering and capture are allowed, and

spin-flip scattering is forbidden. The neutron polarization therefore survives the scattering events that occur before the capture. Higher-energy neutrons will undergo spin-flip scattering and therefore lose their polarization. The liquid-hydrogen target must be in the para- state. For liquid hydrogen held at 20 K and atmospheric pressure, the equilibrium concentration of para-hydrogen is 99.8%, low enough to ensure a negligible population of ortho-hydrogen. The target is under final construction and will be installed in the FP12 cave in the summer of 2005. Production data-taking will begin following this experiment.

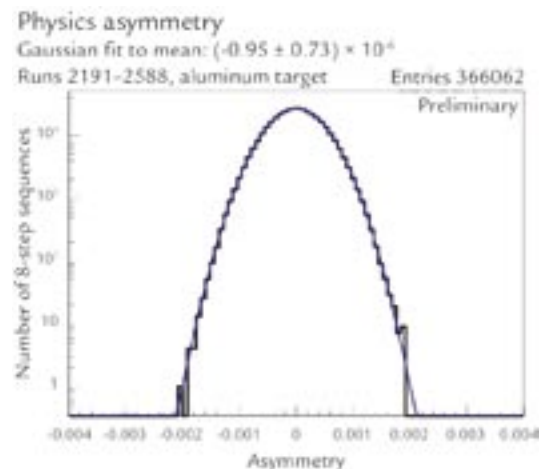## Cesium-Iodide Gamma-Ray Detector Array

Finally, the experiment must detect the 2.2 MeV gamma rays from the neutron capture. Given the small size of the expected asymmetry and the goal precision of the experiment, the number of events required to achieve sufficient statistical accuracy in a reasonable time immediately leads to the conclusion that the 2.2 MeV gamma rays must be counted in current mode. This means that instead of observing individual events in the detector, many are seen at once, and the sum of their presence is detected (as a total voltage or current from the detector electronics, rather than as individual pulses). It is important to demonstrate in a current-mode measurement that the electronic noise is negligible compared to the shot noise due to the discrete nature of the energy deposited by each gamma ray and the number of photoelectrons produced by each event. In addition, the detector must cover a large solid angle with a large and time-independent efficiency that is unaffected by neutron spin reversal and radiation damage. Segmentation of the detector is required to resolve

Figure 4. A photo of the NPDGamma apparatus in the FP12 cave. The neutron beam enters from the left side of the photo. The four horizontal magnetic-field coils are visible surrounding the apparatus. The hydrogen target is not installed.

the angular dependence of the expected parity-violating signal and discriminate false effects. The fully constructed detector array of 48 cesium-iodide scintillator crystals is shown installed in the FP12 cave in Figure 4.[7] The noise performance of the detectors and their preamplifier electronics has been measured in the laboratory, and it corresponds well to predictions based on the fundamental limit of Johnson noise. This allows the detectors to

Figure 5. A histogram of asymmetry values obtained with an aluminum target. The expected asymmetry is zero. The curve is a fit to a Gaussian distribution, and the data are Gaussian to four orders of magnitude.
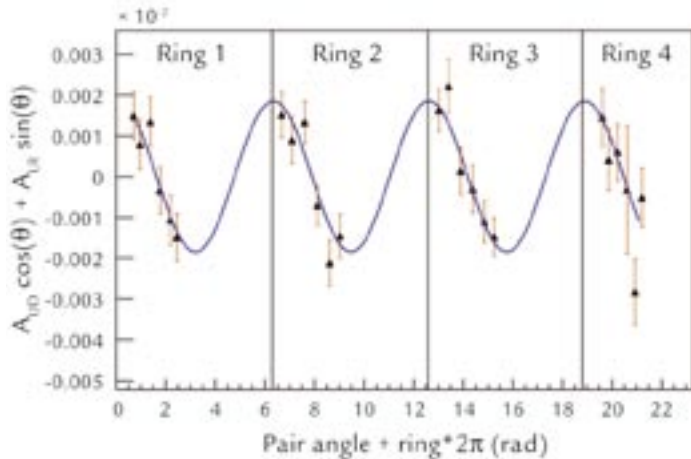
Nuclear Physics and Astrophysics Research Highlights

Figure 6. A plot showing asymmetry results by a detector pair for a chlorine target. Chlorine produces a known gamma-ray asymmetry of ~ 20 parts per million, a result reproduced by this data, shown by the amplitude of the blue fit curve shown on the plot. The data follow a sine and cosine dependence due to the geometry of the detector array. The result of the fit is that $A_{UD} = 19 \pm 2 \times 10^{-6}$, and $A_{LR} = 0.6 \pm 2 \times 10^{-6}$. The notation UD refers to up-down, or the parity-violating direction, while LR is left-right, or parity-conserving direction. No parity-conserving asymmetry is expected.

accumulate data at the counting statistics limit and to quickly demonstrate that no false experimental effects exist in the electronics. As evidence of this, Figure 5 shows a histogram of asymmetry values accumulated with gamma rays produced in an aluminum target. Aluminum is present in much of the experimental apparatus, and if it were to produce a gamma-ray asymmetry, it could obscure the effect we are looking for from our proton target. We have placed a sufficient limit on possible asymmetry arising from neutron capture in aluminum. Figure 6 shows results of gamma-ray asymmetry by a detector pair for a chlorine (CCl_4) target. The sine and cosine dependence of the asymmetry arises due to the physical locations of the detector pairs. Chlorine produces a known asymmetry of ~ 20 parts per million[8], and this shows that our apparatus functions sufficiently to make a precision measurement of a very small asymmetry.

Summary

A sensitive measurement of the parity-violating gamma-ray asymmetry in the reaction $\overline{n} + p \rightarrow d + \gamma$ can give definitive information on one of the most important and interesting components of the weak nucleon-nucleon interaction. Commissioning results have demonstrated the performance of the essential components of the experiment; this includes published results for the FP12 moderator performance and measurements of parity-violating asymmetries in neutron capture on nuclear targets (chlorine, aluminum, and others) to a precision of 2×10^{-6}, limited only by counting statistics. The experimental design incorporates a number of powerful diagnostics to isolate systematic effects. Commissioning of the final assembly of the experiment, including the hydrogen target, will begin in 2005. The NPDGamma experiment to search for the parity-violating gamma-ray asymmetry in the reaction $\overline{n} + p \rightarrow d + \gamma$ will achieve a sensitivity which is likely to obtain a nonzero result, providing an experimental and unambiguous measure of the hadronic weak interaction in a simple and calculable system.

References

1. W.M. Snow *et al.,* "Measurement of the parity violating asymmetry Aγ in $\overline{n} + p \rightarrow d + \gamma$," *Nuclear Instruments and Methods A* **440**, 729–735 (2000).

2. G.E. Mitchell *et al.,* "Parity violation in compound nuclei: Experimental methods and recent results," *Physics Reports* **354**, 157–241 (2001).

3. B. Desplanques, J.F. Donoghue, and B.R. Holstein, "Unified treatment of the parity-violating nuclear force," *Annals of Physics* **124**, 449–495 (1980).

4. E.G. Adelberger and W.C. Haxton, "Parity violation in the nucleon-nucleon interaction," *Annual Review of Nuclear and Particle Science* **35**, 501–558 (1985).

5. S.-L. Zhu *et al.,* "Nuclear parity-violation in effective field theory," ePrint Archives preprint nucl-th/0407087 (29 Dec 04).

6. P.-N. Seo *et al.,* "A measurement of the flight path 12 cold H_2 moderator brightness at LANSCE," *Nuclear Instruments and Methods A* **517**, 285–294 (2004).

7. M. Gericke *et al.,* "A current mode detector array for gamma asymmetry measurements," accepted for publication in *Nuclear Instruments and Methods A* (2005).

8. G.S. Mitchell *et al.,* "A measurement of parity-violating gamma-ray asymmetries in polarized cold neutron capture on ^{35}Cl, ^{113}Cd, and ^{139}La," *Nuclear Instruments and Methods A* **521**, 468–479 (2004).

For further information, contact Gregory Mitchell at 505-665-8484, gmitchell@lanl.gov.

Physics

The World's Greatest Science Protecting America

Los Alamos
NATIONAL LABORATORY
— EST.1943 —